Advances in Nano Research, *Vol. 18, No. 2 (2025) 117-132*
https://doi.org/10.12989/anr.2025.18.2.117

Static response of fully coated porous functionally graded nanoshells

Ali Alnujaie[1,2], Ahmed A. Daikh*[3,4], Mofareh H. Ghazwani[1,2], Amr E. Assie[1,5] and Mohamed A Eltaher[5,6]

[1]*Department of Mechanical Engineering, College of Engineering and Copmuter Sciences, Jazan University, P.O Box 45124, Jazan, Saudi Arabia*
[2]*Engineering and Technology Research Center, P.O. Box 114, Jazan 82817, Saudi Arabia*
[3]*Artificial Intelligence Laboratory for Mechanical and Civil Structures, and Soil, University Centre of Naama, P.O. Box 66, Naama 45000, Algeria*
[4]*Laboratoire d'Etude des Structures et de Mécanique des Matériaux, Département de Génie Civil, Faculté des Sciences et de la Technologie, Université Mustapha Stambouli B.P. 305, R.P.29000 Mascara, Algérie*
[5]*Mechanical Design & Production Department, Faculty of Engineering, Zagazig University, Zagazig 44519, Egypt*
[6]*Mechanical Engineering Department, Faculty of Engineering, King Abdulaziz University, P.O. Box 80204, Jeddah 21589, Saudi Arabia*

(*Received August 14, 2023, Revised February 4, 2025, Accepted February 6, 2025*)

Abstract. The advancement of theoretical research faces numerous challenges, particularly when it comes to modeling structures, in contrast to the experimental investigation of the mechanical behavior of complex systems. Metal foams represent a groundbreaking generation of composite materials, distinguished by their high surface area-to-volume ratio and exceptional properties including porosity, lightweight construction, and heightened thermal conductivity, making them indispensable across industries such as thermal management, filtration, catalysis, and energy storage due to their remarkable versatility and performance capabilities. The study addresses the challenges in theoretical research related to modeling complex structures, presenting a more accurate approach by incorporating nonclassical mechanics. It introduces a novel method for modeling tri-directionally coated porous structures with varying microstructures, accounting for intrinsic characteristic lengths and spatial variations in material properties. The study focuses on the static behavior of multidirectionally functionally graded porous metal foam shells, utilizing higher-order shear deformation theory ansd the principle of virtual work. To tackle various boundary conditions, the investigation employs the Galerkin method, providing a comprehensive and refined analysis of the system's behavior. Two types of porous shells, categorized as Softcore (SC) and Hardcore (HC), are analyzed, with five distribution patterns: tri-directional (Type-A), two bidirectional (Type-B and Type-C), transverse unidirectional (Type-D), and axial unidirectional (Type-E).
Keywords: deflection; higher-order shear deformation theory; Galerkin approach; metal foams; multidirectional material distribution; stresses

1. Introduction

Shell structures, characterized by their curved thin-walled geometry, play a crucial role as complete structures or structural components in various fields, including aerospace, automotive, pressure vessels, marine engineering, and turbomachinery (Punera and Kant 2019). In civil and mechanical engineering, they are widely used in slabs, vaults, roofs, domes, chimneys, cooling towers, pipes, tanks, containers, and pressure vessels (Radwańska *et al*. 2017). Despite extensive research on the static analysis of shell structures, the topic remains an active area of investigation.

Liu *et al*. (2002) applied the Galerkin method to analyze the static and free vibration behavior of thin shell structures. Artioli and Viola (2005) introduced a generalized differential quadrature method (GDQM) to examine the static response of isotropic rotational Reissner-Mindlin shear deformation shells. Asadi and Qatu (2012) extended the use of GDQM to the static analysis of doubly curved composite shells under various boundary conditions. Viola *et al*. (2013) investigated laminated shell structures using higher-order shear deformation theories. Barbero *et al*. (2014) developed a mixed quadrilateral 3D plate element for analyzing the static and buckling behavior of folded laminated composites. Carrera *et al*. (2016) explored reinforced thin-walled plates and shells using a variable kinematic 1D finite element model. Chai *et al*. (2017) introduced the super-convergent alpha finite element method (FEM) with a triangular mesh to study the static and free vibration of shell structures. Zghal and Dammak (2017) employed FEM for the static analysis of functionally graded (FG) carbon nanotube-reinforced shell structures. Hente *et al*. (2021) examined beam and shell structures with singular stiffness matrices caused by redundant coordinates. Pinho *et al*. (2022) utilized Fourier series and the Karhunen–Loève method for the static analysis of shallow shells.

Recent studies have considered structures composed of various material constituents. Medjdoubi *et al*. (2023) developed a novel analytical model to investigate how porosity influences the shear correction factors (SCFs) in functionally graded porous beams (FGPBs). In this study, the porosity distribution across the beam thickness is

*Corresponding author, Ph.D.,
E-mail: daikhresearch@gmail.com

ISSN: 2287-237X (Print), 2287-2388 (Online)

characterized using uneven and logarithmic-uneven functions. Garg *et al*. (2022) attempted to evaluate the stiffness matrix of functionally graded (FG) nannoplates using a Gaussian process regression (GPR)-based surrogate model within the framework of layerwise theory. Abouelregal *et al*. (2021) examined the thermal and mechanical vibration behavior of functionally graded microbeams by formulating the governing equations based on the classical Euler–Bernoulli beam model and the generalized dual-phase lag model of thermoelasticity, instead of the conventional steady-state Fourier heat conduction. Garg *et al*. (2022) investigated the bending behavior of sandwich functionally graded (FGM) beams under thermal loading using shear deformation theory, incorporating temperature-dependent material properties in the analysis. Melaibari *et al*. (2022a, b) investigated the vibration characteristics of composite shells reinforced with randomly oriented single-walled carbon nanotubes and FG fibers. Ladmek *et al*. (2023) developed an analytical method based on higher-order shear deformation theory to study the free vibration behavior of functionally graded carbon nanotube-reinforced composite beams, where material gradation and properties are represented using cosine functions. Tornabene *et al*. (2023) developed a Layer-Wise model for the static analysis of doubly curved shells under general boundary conditions. Abdelhaffez *et al*. (2023) formulated a mathematical model for the buckling of coated FG shells resting on an orthotropic elastic medium. Garg *et al*. (2022) conducted bending and free vibration analyses of multilayered functionally graded graphene platelet (GPL) and fiber-reinforced hybrid composite beams using shear deformation theory based on a parabolic function. Shariati *et al*. (2020) conducted numerical and analytical studies on the size-dependent vibrations and stability of moving viscoelastic axially functionally graded (AFG) nanobeams, with the goal of improving the stability of translating nanosystems, and also provided a parametric analysis to examine the effects of factors such as axial material gradation, viscosity coefficient, and nonlocal parameter on the system's stability boundaries. Garg *et al*. (2023) performed a free vibration analysis of power-law and sigmoidal sandwich plates composed of FGMs using finite element-based higher-order zigzag theory. Chau-Dinh (2023) proposed an enhanced three-node triangular flat shell element with a bubble function and cell-based strain smoothing for static analysis. Sedighi *et al*. (2020) and Sedighi and Malikan (2020) studied instability analysis of fluid-conveying C-BN hybrid-nanotube in a magneto-thermal environment by using stress-driven nonlocal elasticity. Hieu *et al*. (2021) provided a comprehensive theoretical framework for the nonlinear bending, vibration and buckling of functionally graded (FG) nanobeams resting on an elastic foundation through nonlocal strain gradient theory.

Jena *et al*. (2022) investigated the effect of geometrical uncertainties on the free vibration of Euler–Bernoulli FG beams resting on Winkler-Pasternak elastic foundation. Son *et al*. (2024) studied the role of temperature and nonlocality on the low- and high-frequency behaviors of FG sandwich nanoplates resting on Winkler–Pasternak foundations.

Tharwan *et al*. (2023) studied the static behavior of agglomerated coated FG carbon nanotube-reinforced composite nanoshells supported by a complex elastic foundation. A highly efficient nonlocal finite element model is introduced to analyze the bending and buckling behavior of functionally graded (FG) nanobeams, incorporating a newly developed two-node beam element with eight degrees of freedom based on the advanced higher-order shear deformation theory by Belarbi *et al*. (2021). Do *et al*. (2023) provided closed-form solutions for the elastic–plastic buckling of shell structures under external pressure. Khaniki and Ghayesh (2023) applied Donnell's nonlinear shell theory and the Mooney-Rivlin strain energy density model to hyperelastic shell structures. Garg *et al*. (2021) offer an extensive review of sandwich FGM structures, focusing on their use as structural elements and examining various methods and theories for analyzing them under different loading conditions. Daikh *et al*. (2023) evaluated buckling loads and bending deflection in coated FG graphene-reinforced composite plates and shells using the Galerkin technique. Hadji *et al*. (2024) proposed a displacement-based high-order shear deformation theory for the static response of functionally graded plates, which is variationally consistent and closely resembles classical plate theory in many respects, eliminating the need for the shear correction factor. Garg *et al*. (2023) conducted a bending analysis of sandwich functionally graded (FG) beams under thermal conditions using Navier's solution-based parabolic shear deformation theory, presenting a comparative study of exponential and sigmoidal sandwich FGM beams. Rezov (2024) presents a theoretical study on delamination in U-shaped load-carrying structural members, which are multilayered functionally graded systems exhibiting non-linear viscoelastic behavior. The delamination occurs in the right-hand vertical section of the structure, which is clamped at the lower end of the left-hand vertical part and supported by a rotational spring with non-linear elastic behavior. Dang *et al*. (2021) developed a model for a functionally graded (FG) nanotube conveying fluid, embedded in an elastic medium, based on the nonlocal strain gradient theory (NSGT) combined with Euler-Bernoulli beam theory (EBT), aiming to analyze the nonlinear vibrations and stability of fluid-conveying nanotubes.

Metal foams, polymeric foams, and other highly porous materials with cellular structures exhibit unique mechanical and physical properties, such as high stiffness combined with low specific weight, superior gas permeability, and excellent thermal conductivity (Banhart 2001). Hutchinson and He (2000) optimized the face sheet thickness, core thickness, and core density of cylindrical sandwich shells with metal foam cores under buckling constraints. Li *et al*. (2014) performed finite element simulations to analyze the dynamic response of metallic sandwich shells subjected to blast loading. Wang *et al*. (2019) used Love's shell theory to investigate the vibration of metal foam cylindrical shells under different boundary conditions. Toan Thang *et al*. (2020) analyzed the buckling of porous metal foam shells under axial compression. Li *et al*. (2021) examined the vibration characteristics of porous metal foam conical shells

with elastically restrained boundaries using the GDQ method. Ghalambaz *et al*. (2023) explored latent heat thermal energy storage in a metal foam shell-tube system. Xin and Kiani (2023) investigated the vibration of arbitrarily thick sandwich beams with metal foam cores. Song and She (2024) examined the nonlinear vibrations and chaotic dynamic behavior of rotating graphene platelet-reinforced metal foam blades operating in a thermal environment. Ding and She (2024) studied nonlinear combined resonances in axially moving graphene platelet-reinforced metal foam cylindrical shells under forced vibration.

Porous materials are gaining widespread attention due to their favorable properties, such as low specific weight, excellent energy absorption, low thermal and electrical conductivity, high specific strength, and improved recyclability and machinability (Keleshteri and Jelovica 2022). Clausen *et al*. (2017) proposed a 3D topology optimization framework for designing shells with porous interiors. Zhao *et al*. (2019) analyzed the vibration response of FG porous shells with general boundary conditions using first-order shear deformation theory. Ahmadi and Foroutan (2020) developed a semi-analytical model for the static and thermal buckling behavior of multilayer FG cylindrical shells in a thermal environment. Fu *et al*. (2023) examined the dynamic response of stiffened sandwich FG porous doubly curved shells with re-entrant honeycomb auxetic cores. Ramteke and Panda (2023) investigated large geometrical deformation and stress distribution in 2D porous FG shell panels under variable mechanical loads. Sobhy and Radwan (2023) explored the influence of porosity on electro-hygrothermal bending in FG sandwich piezoelectric cylindrical shells using a four-variable shell theory. Ghandourah *et al*. (2023) studied the dynamic behavior of porous coated FG nanoshells resting on a viscoelastic medium. Xue *et al*. (2023) analyzed the free vibration of FG porous shells with porosity variations along thickness and length directions. Houari *et al*. (2024) developed an analytical model to assess the impact of porosity on shear correction factors in FG porous beams.

Coated functionally graded materials are widely used in various industrial applications, including turbine blades, cutting tools, and aircraft engines, due to their superior mechanical properties and ability to withstand extreme conditions. Studying the static response of fully coated functionally graded nanoshells is essential for understanding their behavior under different loading conditions, which is crucial for optimizing their design and ensuring their performance and durability in these high-performance applications.

Despite extensive research, the static analysis of three-dimensional porous metal foam shells has not been thoroughly explored. This study aims to address this gap by presenting a comprehensive analysis of such structures. The proposed approach utilizes nonclassical mechanics to model innovative tri-directionally coated porous structures with varying microstructures, incorporating intrinsic characteristic lengths and spatial variations in material properties for improved accuracy. The proposed model is limited to the static behavior of shells, specifically uniform cross-sectional nanoshells with fixed and hinged boundary conditions.

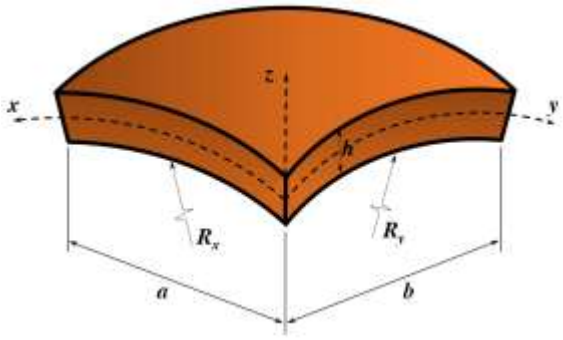

Fig. 1 FG spherical shell geometry

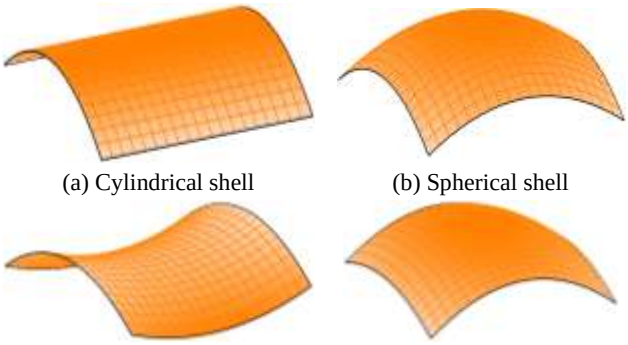

(a) Cylindrical shell (b) Spherical shell

(c) Hyperbolic-Paraboloid shell (d) Elliptical-Paraboloid shell

Fig. 2 Forms of various shells

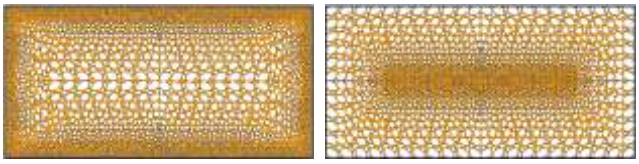

(a) 2D SC surface porosity distribution (b) 2D HC surface porosity distribution

Fig. 3 Porosity distribution through plate surface

2. Geometrical and material distribution

The composite shell under investigation is defined by its dimensions: length (*a*), width (*b*), and thickness (*h*) (Fig. 1). It encompasses various geometrical configurations, including cylindrical, spherical, elliptical–paraboloid, and hyperbolic–paraboloid shells (Fig. 2). The shell's midplane features two principal curvature radii, R_x and R_y, corresponding to the x- and y-directions, respectively.

This structure is composed of porous metal foam, with an analysis of two distinct pore distribution types: hardcore and softcore (Fig. 3). Additionally, five unique pore distribution patterns are considered:

– **FG-A** – A tridirectional material distribution pattern

– **Type-B** – A bidirectional material distribution pattern

– **Type-C** – A second bidirectional material distribution pattern

– **Type-D** – A unidirectional transverse material

distribution pattern

– **Type-E** – A unidirectional axial material distribution pattern

Figs. 4 illustrates these patterns.

– The effective elastic modulus (EEE) and shear modulus (GGG) for both pore distribution types are expressed as follows:

$$\begin{aligned} E(x,y,z) &= E_{max}[1-e_0V(x,y,z)] \\ G(x,y,z) &= G_{max}[1-e_0V(x,y,z)] \end{aligned} \tag{1}$$

where E_{max} and G_{max} represent the maximum values of Young's modulus and shear modulus, respectively. e_0 represents the porosity coefficient, which is calculated as follows:

$$e_0 = 1-\frac{E_{min}}{E_{max}} = 1-\frac{G_{min}}{G_{max}} \tag{2}$$

where E_{min} and G_{min} denote the minimum values of Young's modulus and shear modulus, respectively. The parameter e_0 varies within the range $0<e_0<1$.

The volume fraction V(*x*,*y*,*z*) is defined by three independent functions, each corresponding to a specific spatial direction:

$$\begin{aligned} V(x,y,z) &= V(x)V(y)V(z) \text{ for SC shells} \\ V(x,y,z) &= 1-V(x)V(y)V(z) \text{ for HC shells} \end{aligned} \tag{3}$$

where

$$\begin{aligned} V(x) &= \cos\left(\pi\left(\frac{1}{2}-\frac{x}{a}\right)\right) \\ V(y) &= \cos\left(\pi\left(\frac{1}{2}-\frac{y}{b}\right)\right), \\ V(z) &= \cos\left(\frac{\pi z}{h}\right) \end{aligned} \tag{4}$$

3. Displacement field

The formulations for porous metal foam shells are developed using a shear deformation theory based on an inverse trigonometric function. The displacement field is expressed as follows (Daikh *et al*. 2023):

$$\begin{aligned} u(x,y,z,t) &= \left(1+\frac{z}{R_x}\right)u_0 - z\frac{\partial w_0}{\partial x} + f(z)\psi_x \\ v(x,y,z,t) &= \left(1+\frac{z}{R_y}\right)v_0 - z\frac{\partial w_0}{\partial y} + f(z)\psi_y \\ w(x,y,z,t) &= w_0 \end{aligned}, \tag{5}$$

The midplane displacements of the shell are denoted as u_0, v_0, and w_0, while the transverse normal rotations at $z=0$ are represented by ψ_x and ψ_y. The shape function $f(z)$ is defined as:

$$f(z) = 5h\,\text{atan}\left(\frac{z}{h}\right) - 4z \tag{6}$$

The strains can be determined by differentiating the displacement equation provided earlier:

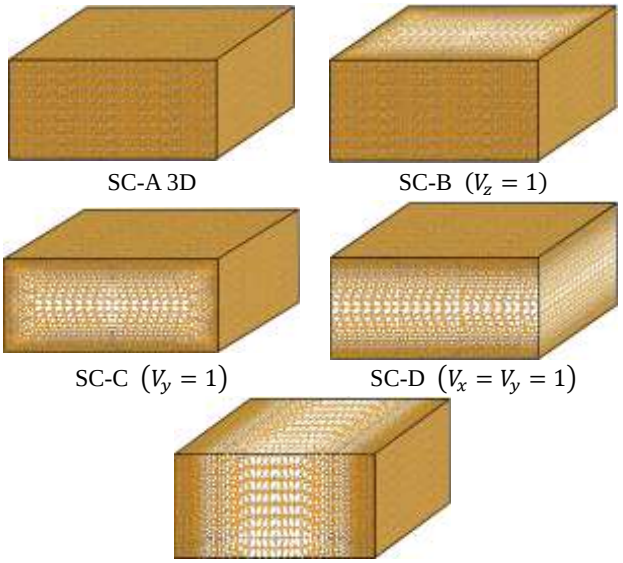

Fig. 4 Various schemes of SC porous shell ($R_x=R_y=\infty$)

$$\begin{Bmatrix}\varepsilon_{xx}\\ \varepsilon_{yy}\\ \gamma_{xy}\end{Bmatrix} = \begin{Bmatrix}\varepsilon^0_{xx}\\ \varepsilon^0_{yy}\\ \gamma^0_{xy}\end{Bmatrix} + z\begin{Bmatrix}\varepsilon^1_{xx}\\ \varepsilon^1_{yy}\\ \gamma^1_{xy}\end{Bmatrix} + f(z)\begin{Bmatrix}\varepsilon^2_{xx}\\ \varepsilon^2_{yy}\\ \gamma^2_{xy}\end{Bmatrix}, \varepsilon_{zz}=0, \quad \begin{Bmatrix}\gamma_{yz}\\ \gamma_{xz}\end{Bmatrix} = \frac{\mathrm{d}f(z)}{\mathrm{d}z}\begin{Bmatrix}\gamma^0_{yz}\\ \gamma^0_{xz}\end{Bmatrix} \tag{7}$$

where

$$\begin{Bmatrix}\varepsilon^0_{xx}\\ \varepsilon^0_{yy}\\ \gamma^0_{xy}\end{Bmatrix} = \begin{Bmatrix}\frac{\partial u_0}{\partial x}+\frac{w_0}{R_x}\\ \frac{\partial v_0}{\partial y}+\frac{w_0}{R_y}\\ \frac{\partial v_0}{\partial x}+\frac{\partial u_0}{\partial y}\end{Bmatrix}, \quad \begin{Bmatrix}\varepsilon^1_{xx}\\ \varepsilon^1_{yy}\\ \gamma^1_{xy}\end{Bmatrix} = -\begin{Bmatrix}\frac{\partial^2 w_0}{\partial x^2}\\ \frac{\partial^2 w_0}{\partial y^2}\\ 2\frac{\partial^2 w_0}{\partial x\partial y}\end{Bmatrix}, \quad \begin{Bmatrix}\varepsilon^2_{xx}\\ \varepsilon^2_{yy}\\ \gamma^2_{xy}\end{Bmatrix} = \begin{Bmatrix}\frac{\partial \varphi_1}{\partial x}\\ \frac{\partial \varphi_2}{\partial y}\\ \frac{\partial \varphi_2}{\partial x}+\frac{\partial \varphi_1}{\partial y}\end{Bmatrix}, \quad \begin{Bmatrix}\gamma^0_{yz}\\ \gamma^0_{xz}\end{Bmatrix} = \begin{Bmatrix}\varphi_x\\ \varphi_y\end{Bmatrix}. \tag{8}$$

The stress-strain relationships based on the nonlocal strain gradient constitutive theory are given by:

$$\begin{Bmatrix}\sigma_{xx}\\ \sigma_{yy}\\ \tau_{yz}\\ \tau_{xz}\\ \tau_{xy}\end{Bmatrix} = \begin{bmatrix}Q_{11} & Q_{12} & 0 & 0 & 0\\ Q_{12} & Q_{22} & 0 & 0 & 0\\ 0 & 0 & Q_{44} & 0 & 0\\ 0 & 0 & 0 & Q_{55} & 0\\ 0 & 0 & 0 & 0 & Q_{66}\end{bmatrix}\begin{Bmatrix}\varepsilon_{xx}\\ \varepsilon_{yy}\\ \gamma_{yz}\\ \gamma_{xz}\\ \gamma_{xy}\end{Bmatrix} \tag{9}$$

where

$$Q_{11} = \frac{E}{1-\nu^2}, Q_{22} = Q_{11}, \quad Q_{12} = \frac{\nu E}{1-\nu^2}, \quad Q_{44} = Q_{55} = Q_{66} = \frac{E}{2(1+\nu)} \tag{10}$$

Integrating Eq. (32) yields the expressions for the stress resultants, moments, and additional moment resultants as follows:

$$\begin{Bmatrix}\{N\}\\\{M\}\\\{P\}\end{Bmatrix}=\begin{bmatrix}[A] & [B] & [C]\\ [B] & [D] & [F]\\ [C] & [F] & [H]\end{bmatrix}\begin{Bmatrix}\{\varepsilon^0\}\\\{\varepsilon^1\}\\\{\varepsilon^2\}\end{Bmatrix} \tag{11}$$

$$\begin{Bmatrix}R_{yz}\\R_{xz}\end{Bmatrix}=\begin{bmatrix}J_{44} & J_{45}\\ J_{45} & J_{55}\end{bmatrix}\begin{Bmatrix}\gamma^0_{yz}\\\gamma^0_{xz}\end{Bmatrix} \tag{12}$$

where

$$\begin{aligned}&\{N\}=\{N_{xx}\quad N_{yy}\quad N_{xy}\}^T,\\&\{M\}=\{M_{xx}\quad M_{yy}\quad M_{xy}\}^T,\\&\{P\}=\{P_{xx}\quad P_{yy}\quad P_{xy}\}^T,\\&\{\varepsilon^0\}=\{\varepsilon^0_{xx}\quad \varepsilon^0_{yy}\quad \gamma^0_{xy}\}^T,\\&\{\varepsilon^1\}=\{\varepsilon^1_{xx}\quad \varepsilon^1_{yy}\quad \gamma^1_{xy}\}^T,\\&\{\varepsilon^2\}=\{\varepsilon^2_{xx}\quad \varepsilon^2_{yy}\quad \gamma^2_{xy}\}^T\end{aligned} \tag{13}$$

and

$$\begin{aligned}&\{A_{ij},B_{ij},D_{ij},C_{ij},F_{ij},H_{ij}\}=\\&\int_{-h/2}^{h/2}Q_{ij}\{1,z,z^2,f(z),zf(z),f(z)^2\}\mathrm{d}z,(i,j=1,2,6)\\&J_{ii}=\int_{-h/2}^{h/2}Q_{ii}\left[\frac{\mathrm{d}f(z)}{\mathrm{d}z}\right]^2\mathrm{d}z,(i=4,5)\end{aligned} \tag{14}$$

4. Equilibrium equations

To derive the equilibrium equations, the potential energy principle is employed, given by

$$\int_V\sigma_{ij}\delta\varepsilon_{ij}\mathrm{d}V-\int_A q\delta w\mathrm{d}A=0 \tag{15}$$

e symbol q denotes the distributed transverse load. By integrating the strains and stresses, the potential energy principle is formulated as:

$$\begin{aligned}\delta U=\int_A\Bigg[&N_{xx}\frac{\partial u}{\partial x}-M_{xx}\frac{\partial^2 w}{\partial x^2}-S_{xx}\frac{\partial^2\psi}{\partial x^2}\\&+N_{yy}\frac{\partial v}{\partial y}-M_{yy}\frac{\partial^2 w}{\partial y^2}-\\&S_{yy}\frac{\partial^2\psi}{\partial y^2}+N_{xy}\left(\frac{\partial u}{\partial y}+\frac{\partial v}{\partial x}\right)\\&-2M_{xy}\frac{\partial^2 w}{\partial x\partial y}-2S_{xy}\frac{\partial^2\psi}{\partial x\partial y}-q\delta w\Bigg]\end{aligned} \tag{16}$$

Substituting Eqs. (8,9,11) into Eqs. (16) yields the equilibrium equations for the shell, as follows:

$$\begin{aligned}&A_{11}\frac{\partial^2 u_0}{\partial x^2}+A_{66}\frac{\partial^2 u_0}{\partial y^2}+(A_{12}+A_{66})\frac{\partial^2 v_0}{\partial x\partial y}\\&+\left(\frac{A_{11}}{R_x}+\frac{A_{12}}{R_y}\right)\frac{\partial w_0}{\partial x}-B_{11}\frac{\partial^3 w_0}{\partial x^3}\\&-(B_{12}+2B_{66})\frac{\partial^3 w_0}{\partial x\partial y^2}+B^s_{11}\frac{\partial^2\psi_x}{\partial x^2}\\&+B^s_{66}\frac{\partial^2\psi_x}{\partial y^2}+(B^s_{12}+B^s_{66})\frac{\partial^2\psi_y}{\partial x\partial y}=0\end{aligned} \tag{17}$$

$$\begin{aligned}&(A_{12}+A_{66})\frac{\partial^2 u_0}{\partial x\partial y}+A_{22}\frac{\partial^2 v_0}{\partial y^2}+A_{66}\frac{\partial^2 v_0}{\partial x^2}\\&-(B_{12}+2B_{66})\frac{\partial^3 w_0}{\partial x^2\partial y}-B_{22}\frac{\partial^3 w_0}{\partial y^3}\\&\left(\frac{A_{12}}{R_x}+\frac{A_{22}}{R_y}\right)\frac{\partial w_0}{\partial x}+(B^s_{12}+B^s_{66})\frac{\partial^2\psi_x}{\partial x\partial y}\\&+B^s_{22}\frac{\partial^2\psi_y}{\partial y^2}+B^s_{66}\frac{\partial^2\psi_y}{\partial x^2}=0\end{aligned} \tag{18}$$

$$\begin{aligned}&B_{11}\frac{\partial^3 u_0}{\partial x^3}+(B_{12}+2B_{66})\frac{\partial^3 u_0}{\partial x\partial y^2}-\left(\frac{A_{11}}{R_x}+\frac{A_{12}}{R_y}\right)\frac{\partial u_0}{\partial x}\\&+(B_{12}+2B_{66})\frac{\partial^3 v_0}{\partial x^2\partial y}+B_{22}\frac{\partial^3 v_0}{\partial y^3}-\left(\frac{A_{12}}{R_x}+\frac{A_{22}}{R_y}\right)\frac{\partial v_0}{\partial y}\\&+\left(\frac{2B_{11}}{R_x}+\frac{2B_{12}}{R_y}\right)\frac{\partial^2 w_0}{\partial x^2}-D_{11}\frac{\partial^4 w_0}{\partial x^4}\\&-(2D_{12}+4D_{66})\frac{\partial^4 w_0}{\partial x^2\partial y^2}-D_{22}\frac{\partial^4 w_0}{\partial y^4}\\&+\left(\frac{2B_{12}}{R_x}+\frac{2B_{22}}{R_y}\right)\frac{\partial^2 w_0}{\partial y^2}-\left(\frac{A_{11}}{{R_x}^2}+2\frac{A_{12}}{R_xR_y}+\frac{A_{22}}{{R_y}^2}\right)w_0\\&+D^s_{11}\frac{\partial^3\psi_x}{\partial x^3}+(D^s_{12}+2D^s_{66})\frac{\partial^3\psi_x}{\partial x\partial y^2}\\&-\left(\frac{B^s_{11}}{R_x}+\frac{B^s_{12}}{R_y}\right)\frac{\partial\psi_x}{\partial x}+(D^s_{12}+2D^s_{66})\frac{\partial^3\psi_y}{\partial x^2\partial y}\\&+D^s_{22}\frac{\partial^3\psi_y}{\partial y^3}-\left(\frac{B^s_{12}}{R_x}+\frac{B^s_{22}}{R_y}\right)\frac{\partial\psi_y}{\partial y}+q=0\end{aligned} \tag{19}$$

$$\begin{aligned}&B^s_{11}\frac{\partial^2 u_0}{\partial x^2}+B^s_{66}\frac{\partial^2 u_0}{\partial y^2}+(B^s_{12}+B^s_{66})\frac{\partial^2 v_0}{\partial x\partial y}-D^s_{11}\frac{\partial^3 w_0}{\partial x^3}\\&-(D^s_{12}+2D^s_{66})\frac{\partial^3 w_0}{\partial x\partial y^2}+\left(\frac{B^s_{11}}{R_x}+\frac{B^s_{12}}{R_y}\right)\frac{\partial w_0}{\partial x}+F^s_{11}\frac{\partial^2\psi_x}{\partial x^2}\\&+F^s_{66}\frac{\partial^2\psi_x}{\partial y^2}-A^s_{44}\psi_x+(F^s_{12}+F^s_{66})\frac{\partial^2\psi_y}{\partial x\partial y}=0\end{aligned} \tag{20}$$

$$\begin{aligned}&(B^s_{12}+B^s_{66})\frac{\partial^2 u_0}{\partial x\partial y}+B^s_{11}\frac{\partial^2 v_0}{\partial y^2}+B^s_{66}\frac{\partial^2 v_0}{\partial x^2}\\&-(D^s_{12}+2D^s_{66})\frac{\partial^3 w_0}{\partial x^2\partial y}-D^s_{22}\frac{\partial^3 w_0}{\partial y^3}\\&+\left(\frac{B^s_{12}}{R_x}+\frac{B^s_{22}}{R_y}\right)\frac{\partial w_0}{\partial x}+(F^s_{12}+F^s_{66})\frac{\partial^2\psi_x}{\partial x\partial y}\\&+F^s_{11}\frac{\partial^2\psi_y}{\partial y^2}+F^s_{66}\frac{\partial^2\psi_y}{\partial x^2}-A^s_{44}\psi_y=0\end{aligned} \tag{21}$$

5. Analytical solution

One of the primary objectives of this research is to extend the application of analytical solutions for evaluating the response of various structural forms, including shell

Table 1 The admissible functions $X_m(x)$ and $Y_n(y)$

BCs.	The functions X_m and Y_n	
	$X_m(x)$	$Y_n(y)$
SSSS	$\sin(\alpha x)$	$\sin(\beta y)$
CCCC	$\sin^2(\alpha x)$	$\sin^2(\beta y)$
CSCS	$\sin(\alpha x)[\cos(\alpha x)-1]$	$\sin(\beta y)[\cos(\beta y)-1]$
CCSS	$\sin^2(\alpha x)$	$\sin(\beta y)$

Table 2 Dimensionless central deflection $\bar{w}$ of porous shells (SSSS, a=b=10h)

Shell	e_0	SC-A	SC-B	SC-C	SC-D	SC-E	HC-A	HC-B	HC-C	HC-D	HC-E
plate	0.2	2.99310	3.15508	3.04963	3.14335	3.32236	3.48830	3.29075	3.41547	3.30733	3.12657
	0.4	3.09371	3.46030	3.21816	3.43861	3.88989	4.37903	3.80434	4.15807	3.85398	3.39244
	0.6	3.20211	3.83090	3.40935	3.81067	4.69128	5.88516	4.50789	5.31995	4.62521	3.70773
	0.8	3.31947	4.29041	3.62988	4.32180	5.90853	8.99007	5.53069	7.40170	5.79659	4.08763
Cylindrical	0.2	2.91048	3.06618	2.96650	3.05942	3.22874	3.38766	3.19803	3.31570	3.20892	3.03847
	0.4	3.01019	3.36280	3.13366	3.35268	3.78029	4.24821	3.69715	4.03035	3.73109	3.29685
	0.6	3.11773	3.72296	3.32359	3.72299	4.55909	5.69908	4.38087	5.14394	4.46377	3.60326
	0.8	3.23427	4.16952	3.54297	4.23205	5.74205	8.67319	5.37485	7.12523	5.56767	3.97246
Spherical	0.2	2.68790	2.82720	2.74223	2.83254	2.97709	3.11782	2.94877	3.04853	2.94593	2.80165
	0.4	2.78467	3.10070	2.90485	3.11887	3.48565	3.89879	3.40899	3.69030	3.40532	3.03989
	0.6	2.88933	3.43279	3.09039	3.48260	4.20375	5.20532	4.03942	4.67949	4.04065	3.32242
	0.8	3.00304	3.84454	3.30554	3.98385	5.29451	7.84374	4.95593	6.40725	4.97792	3.66284
Hyperbolic-paraboloid	0.2	2.76263	2.90736	2.81758	2.90885	3.06150	3.20822	3.03238	3.13797	3.03388	2.88108
	0.4	2.86048	3.18862	2.98187	3.19776	3.58448	4.01563	3.50564	3.80383	3.51385	3.12608
	0.6	2.96620	3.53012	3.16905	3.56400	4.32294	5.36989	4.15395	4.83388	4.18083	3.41662
	0.8	3.08096	3.95355	3.38580	4.06825	5.44462	8.11838	5.09644	6.64408	5.17170	3.76669
Elliptical-paraboloid	0.2	2.99310	3.15508	3.04963	3.14335	3.32236	3.48830	3.29075	3.41547	3.30733	3.12657
	0.4	3.09371	3.46030	3.21816	3.43861	3.88989	4.37903	3.80434	4.15807	3.85398	3.39244
	0.6	3.20211	3.83090	3.40935	3.81067	4.69128	5.88516	4.50789	5.31995	4.62521	3.70773
	0.8	3.31947	4.29041	3.62988	4.32180	5.90853	8.99007	5.53069	7.40170	5.79659	4.08763

structures, under different boundary conditions. To accomplish this, the Galerkin method is utilized to derive precise solutions. The generalized displacements are expressed as follows:

$$\begin{aligned}\{u_0,\psi_x\} &= \sum_{m=1}^{\infty}\sum_{n=1}^{\infty}\{U_{mn},X_{mn}\}\frac{\partial X_m(x)}{\partial x}Y_n(y)\\ \{v_0,\psi_y\} &= \sum_{m=1}^{\infty}\sum_{n=1}^{\infty}\{V_{mn},Z_{mn}\}X_m(x)\frac{\partial Y_n(y)}{\partial y}\\ w_0 &= \sum_{m=1}^{\infty}\sum_{n=1}^{\infty}W_{mn}X_m(x)Y_n(y)\end{aligned} \tag{22}$$

U_{mn}, V_{mn}, W_{mn}, X_{mn} and Z_{mn} are arbitrary parameters. Table 2 contains the functions $X_m(x)$ and $Y_n(y)$ that satisfy the above boundary conditions.

The parameters U_{mn}, V_{mn}, W_{mn}, X_{mn} and Z_{mn} are arbitrary. Table 1 presents the functions $X_m(x)$ and $Y_n(y)$ that meet the aforementioned boundary conditions, where $\lambda = m\pi/a$, $\mu = n\pi/b$. m and n are mode numbers.

The transverse sinusoidal load that is applied can be defined as follows:

$$q = -q_0\int_0^a\int_0^b \sin^2(\alpha x)\sin^2(\beta y)\,\mathrm{d}x\mathrm{d}y \tag{23}$$

where q_0 is the maximum load intensity. By substituting Eq. (22) in Eqs. (17-21), one obtains

$$[K]_{5\times5}\begin{Bmatrix}U_{mn}\\V_{mn}\\W_{mn}\\\Psi_{mn}\\\Phi_{mn}\end{Bmatrix} = \begin{Bmatrix}0\\0\\q_0\\0\\0\end{Bmatrix} \tag{24}$$

where [K] and [M] are the rigidity matrix and mass matrix, respectively. The elements K_{ij} and M_{ij} of the matrix [K] and [M] are given in Appendix A.

6. Results and discussions

A detailed numerical analysis is conducted to investigate

Table 3 Dimensionless axial stress $\bar{\sigma}_{xx}$ of porous shells (SSSS, a=b=10h)

Shell	e_0	SC-A	SC-B	SC-C	SC-D	SC-E	HC-A	HC-B	HC-C	HC-D	HC-E
plate	0.2	2.11004	1.78260	2.14741	2.20892	1.87711	1.97470	2.32407	1.93537	1.87667	2.20812
	0.4	2.17641	1.46629	2.25758	2.39837	1.64833	1.86411	2.68679	1.77348	1.64771	2.39589
	0.6	2.24718	1.08222	2.37993	2.62482	1.32527	1.67653	3.18366	1.51956	1.32482	2.61856
	0.8	2.32280	0.60601	2.51679	2.90307	0.83457	1.28814	3.90601	1.06333	0.83460	2.88686
Cylindrical	0.2	2.19732	1.85502	2.23720	2.30291	1.95337	2.05324	2.41849	2.01146	1.94919	2.29782
	0.4	2.26817	1.52586	2.35498	2.50607	1.71529	1.93587	2.79594	1.83991	1.70710	2.49322
	0.6	2.34385	1.12619	2.48624	2.75058	1.37911	1.73750	3.31300	1.57216	1.36785	2.72494
	0.8	2.42489	0.63063	2.63368	3.05438	0.86848	1.32947	4.06470	1.09486	0.85731	3.00414
Spherical	0.2	2.16367	1.82353	2.20518	2.27376	1.92021	2.01440	2.37743	1.97132	1.90728	2.25881
	0.4	2.23748	1.49995	2.32827	2.48724	1.68617	1.89361	2.74847	1.79538	1.66021	2.45089
	0.6	2.31660	1.10707	2.46631	2.74710	1.35570	1.69108	3.25675	1.52380	1.31901	2.67868
	0.8	2.40167	0.61993	2.62247	3.07445	0.85373	1.28077	3.99569	1.04861	0.81628	2.95314
Hyperbolic-paraboloid	0.2	2.18437	1.84200	2.22552	2.29346	1.93966	2.03614	2.40152	1.99329	1.92955	2.28170
	0.4	2.25752	1.51515	2.34740	2.50447	1.70325	1.91594	2.77632	1.81801	1.68301	2.47572
	0.6	2.33586	1.11828	2.48381	2.76040	1.36943	1.71386	3.28975	1.54645	1.34088	2.70582
	0.8	2.41998	0.62621	2.63778	3.08146	0.86238	1.30241	4.03617	1.06839	0.83328	2.98306
Elliptical-paraboloid	0.2	2.11004	1.78260	2.14741	2.20892	1.87711	1.97470	2.32407	1.93537	1.87667	2.20812
	0.4	2.17641	1.46629	2.25758	2.39837	1.64833	1.86411	2.68679	1.77348	1.64771	2.39589
	0.6	2.24718	1.08222	2.37993	2.62482	1.32527	1.67653	3.18366	1.51956	1.32482	2.61856
	0.8	2.32280	0.60601	2.51679	2.90307	0.83457	1.28814	3.90601	1.06333	0.83460	2.88686

Table 4 Dimensionless shear stress $\bar{\tau}_{xz}$ of porous shells (SSSS, a=b=10h)

Shell	e_0	SC-A	SC-B	SC-C	SC-D	SC-E	HC-A	HC-B	HC-C	HC-D	HC-E
plate	0.2	0.26383	0.26805	0.27502	0.23575	0.28227	0.22751	0.22366	0.21803	0.25583	0.21250
	0.4	0.28409	0.29399	0.31148	0.22049	0.33048	0.20192	0.19393	0.18317	0.26658	0.17293
	0.6	0.30779	0.32547	0.35942	0.19595	0.39857	0.16502	0.15319	0.13907	0.27912	0.12600
	0.8	0.33593	0.36451	0.42537	0.14804	0.50199	0.10698	0.09398	0.08114	0.29449	0.06946
Cylindrical	0.2	0.25655	0.26050	0.26752	0.22946	0.27431	0.22095	0.21736	0.21166	0.24821	0.20652
	0.4	0.27642	0.28570	0.30331	0.21498	0.32117	0.19589	0.18846	0.17755	0.25808	0.16806
	0.6	0.29968	0.31630	0.35038	0.19144	0.38734	0.15980	0.14888	0.13447	0.26937	0.12245
	0.8	0.32731	0.35424	0.41519	0.14496	0.48784	0.10321	0.09133	0.07811	0.28286	0.06750
Spherical	0.2	0.23693	0.24020	0.24730	0.21244	0.25293	0.20335	0.20042	0.19461	0.22787	0.19042
	0.4	0.25571	0.26343	0.28116	0.19999	0.29614	0.17977	0.17378	0.16257	0.23555	0.15496
	0.6	0.27773	0.29165	0.32580	0.17908	0.35715	0.14595	0.13727	0.12233	0.24384	0.11291
	0.8	0.30391	0.32663	0.38737	0.13646	0.44982	0.09334	0.08421	0.07024	0.25290	0.06224
Hyperbolic-paraboloid	0.2	0.24352	0.24701	0.25409	0.21817	0.26010	0.20925	0.20610	0.20032	0.23468	0.19582
	0.4	0.26267	0.27090	0.28861	0.20505	0.30454	0.18516	0.17870	0.16757	0.24305	0.15935
	0.6	0.28512	0.29992	0.33409	0.18327	0.36727	0.15057	0.14117	0.12636	0.25230	0.11611
	0.8	0.31179	0.33589	0.39677	0.13935	0.46257	0.09661	0.08660	0.07283	0.26275	0.06400
Elliptical-paraboloid	0.2	0.26383	0.26805	0.27502	0.23575	0.28227	0.22751	0.22366	0.21803	0.25583	0.21250
	0.4	0.28409	0.29399	0.31148	0.22049	0.33048	0.20192	0.19393	0.18317	0.26658	0.17293
	0.6	0.30779	0.32547	0.35942	0.19595	0.39857	0.16502	0.15319	0.13907	0.27912	0.12600
	0.8	0.33593	0.36451	0.42537	0.14804	0.50199	0.10698	0.09398	0.08114	0.29449	0.06946

the static behavior of multidirectional porous metal foam shells. The study focuses on the effects of key parameters, including porosity distribution, porosity coefficient, shell geometry, and different boundary conditions. The results

Table 5 Dimensionless central deflection $\bar{w}$ of porous spherical shells (e_0=0.5 a=b=10h)

BCs.	a/h	SC-A	SC-B	SC-C	SC-D	SC-E	HC-A	HC-B	HC-C	HC-D	HC-E
SSSS	5	3.60587	4.10381	3.83697	4.29099	4.80014	5.55565	4.65700	5.12421	4.57347	3.99874
	10	2.83595	3.25831	2.99440	3.28864	3.81117	4.45788	3.69752	4.12585	3.69520	3.17488
	20	2.11673	2.41198	2.24603	2.48546	2.82124	3.25311	2.73711	2.99020	2.65359	2.35022
	30	1.53935	1.73488	1.64536	1.84520	2.02925	2.30059	1.96874	2.09886	1.84482	1.69046
CCCC	5	2.43601	2.72147	2.62815	3.02616	3.18324	3.59600	3.08832	3.28581	2.90063	2.65179
	10	1.62331	1.85454	1.72198	1.91187	2.16922	2.52134	2.10453	2.32875	2.08132	1.80706
	20	1.24136	1.42052	1.31386	1.44827	1.66155	1.92993	1.61201	1.78015	1.58710	1.38415
	30	0.98337	1.11679	1.04579	1.16215	1.30628	1.49860	1.26733	1.37440	1.21620	1.08819
CCSS	5	2.64468	2.97082	2.84171	3.24413	3.47490	3.95383	3.37128	3.62290	3.20873	2.89475
	10	1.85780	2.12675	1.96755	2.17661	2.48761	2.89847	2.41343	2.67940	2.39700	2.07229
	20	1.42838	1.63381	1.51211	1.66703	1.91103	2.21769	1.85405	2.04461	1.82167	1.59198
	30	1.11609	1.26584	1.18796	1.32211	1.48062	1.69501	1.43647	1.55305	1.37258	1.23343
CSCS	5	0.86767	0.97512	0.93209	1.06375	1.14058	1.29886	1.10657	1.19061	1.05507	0.95015
	10	0.62161	0.71261	0.65771	0.72632	0.83352	0.97332	0.80867	0.90064	0.80675	0.69436
	20	0.50200	0.57614	0.53024	0.58221	0.67390	0.78619	0.65381	0.72656	0.64935	0.56139
	30	0.41417	0.47208	0.43939	0.48604	0.55218	0.63695	0.53571	0.58557	0.51976	0.45999

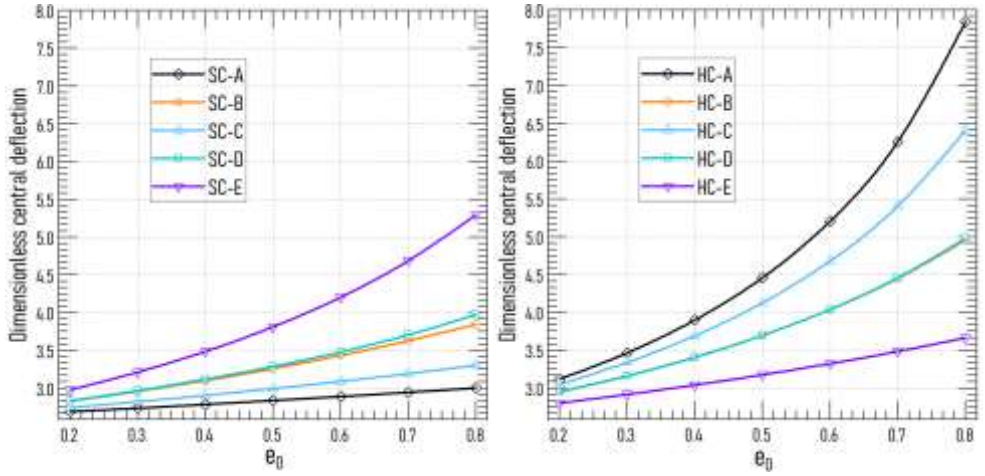

Fig. 5 Dimensionless central deflection $\bar{w}$ versus porosity coefficient e_0 of various patterns of porous spherical shells (SSSS, a=b=10h)

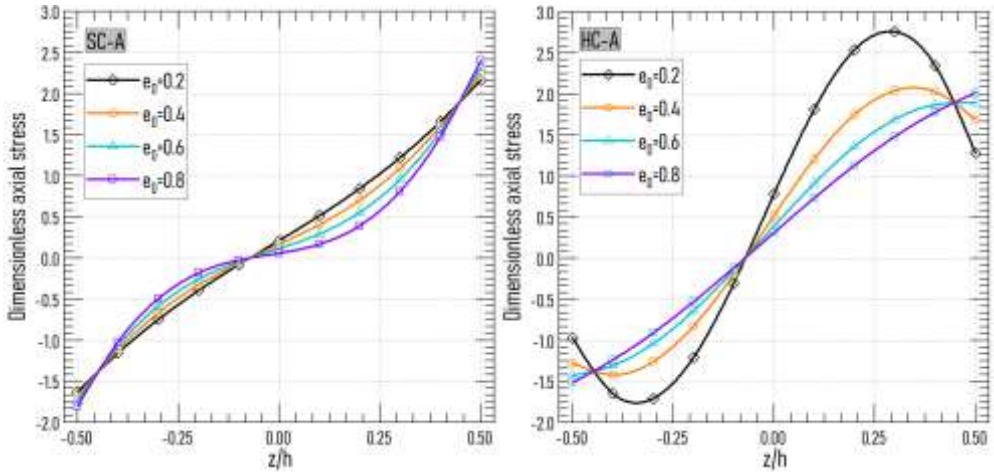

Fig. 6 Effect of porosity coefficient e_0 on the dimensionless axial stress $\bar{\sigma}_{xx}$ 3D porous spherical shells (SSSS, a=b=10h)

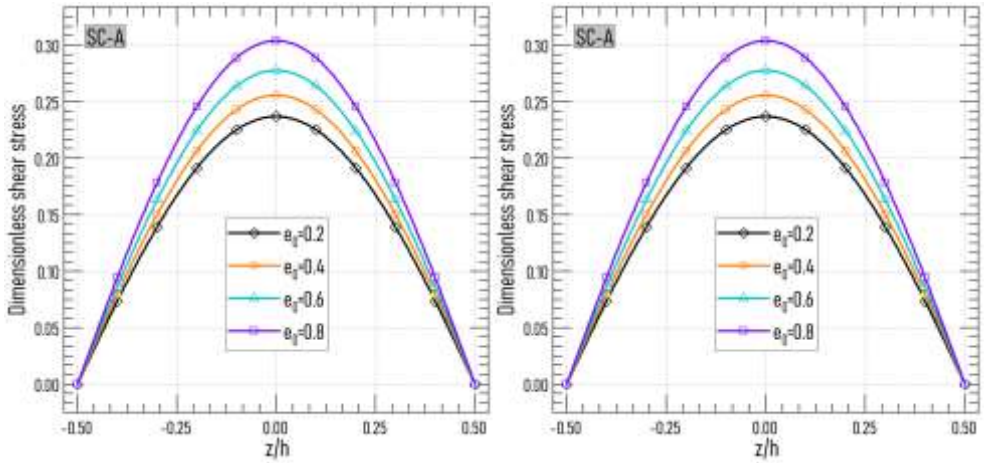

Fig. 7 Effect of porosity coefficient e_0 on the dimensionless shear stress $\bar{\tau}_{xz}$ 3D porous spherical shells (SSSS, a=b=10h)

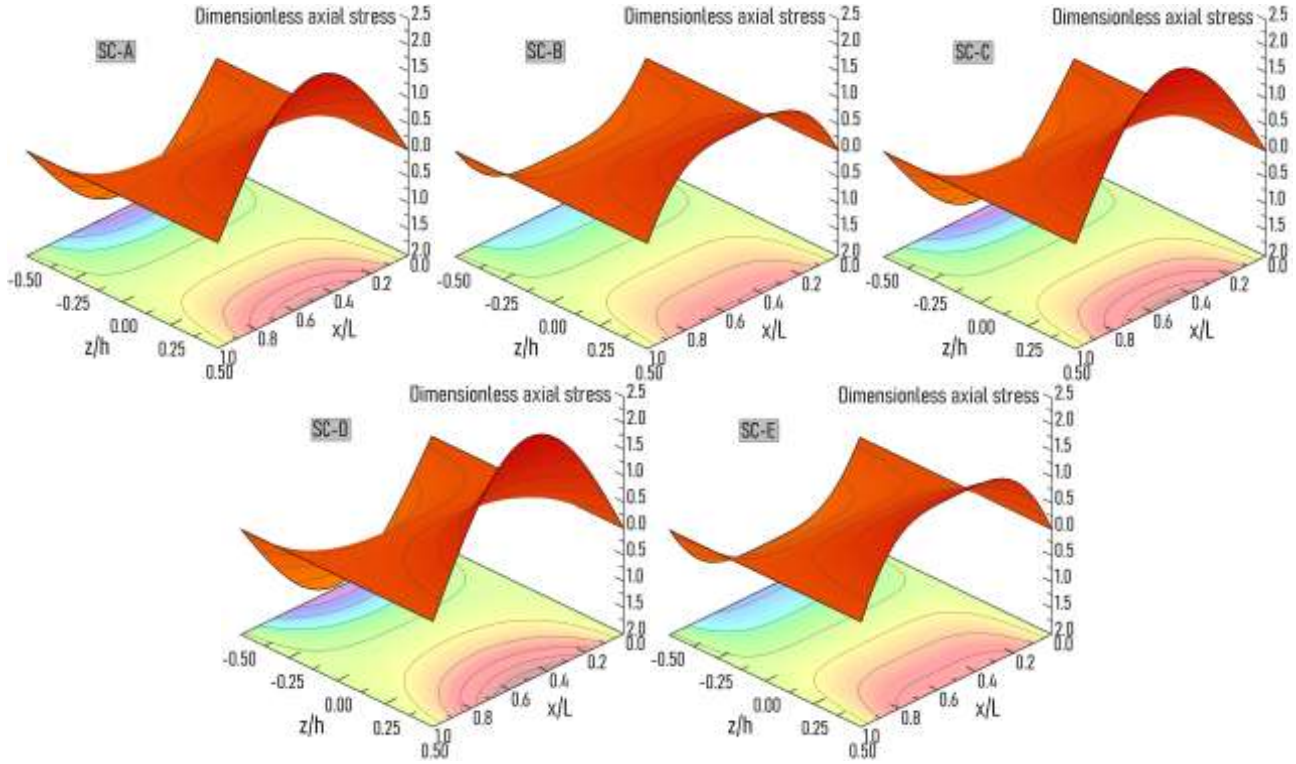

Fig. 8 Dimensionless axial stress "$\bar{\sigma}_{xx}$" distribution of various SC porous spherical shell patterns (SSSS, $e_0 = 0.3$, $a = b = 10h$)

are systematically presented in tables and graphs.

The porous beams are assumed to be made of open-cell steel foam, characterized by the following material properties: $E_{max} = 200$ GPa and $\upsilon = 1/3$.

The normalized results for stresses and deflection are calculated using the following expressions:

$$\bar{w} = \frac{10E_{max}h^3}{a^2 q_0} w\left(\frac{a}{2}, \frac{b}{2}, z\right) \tag{25}$$

$$\bar{\sigma}_{xx} = \frac{ah}{q_0}\sigma_{xx}\left(\frac{a}{2}, \frac{b}{2}, \frac{h}{2}\right) \tag{26}$$

$$\bar{\tau}_{xz} = \frac{ah}{q_0}\tau_{xz}\left(0, \frac{b}{2}, 0\right) \tag{27}$$

Numerical results are collected to evaluate the effects of the porosity coefficient and distribution schemes on the central deflection (Table 2), axial stress (Table 3), and shear stress (Table 4). Furthermore, the study examines the influence of various boundary conditions and thickness ratios on deflections, with the findings summarized in Table 5.

To provide a clearer understanding, Figs. 6-15 are presented and thoroughly discussed, offering an in-depth analysis of the static response of porous functionally graded shells.

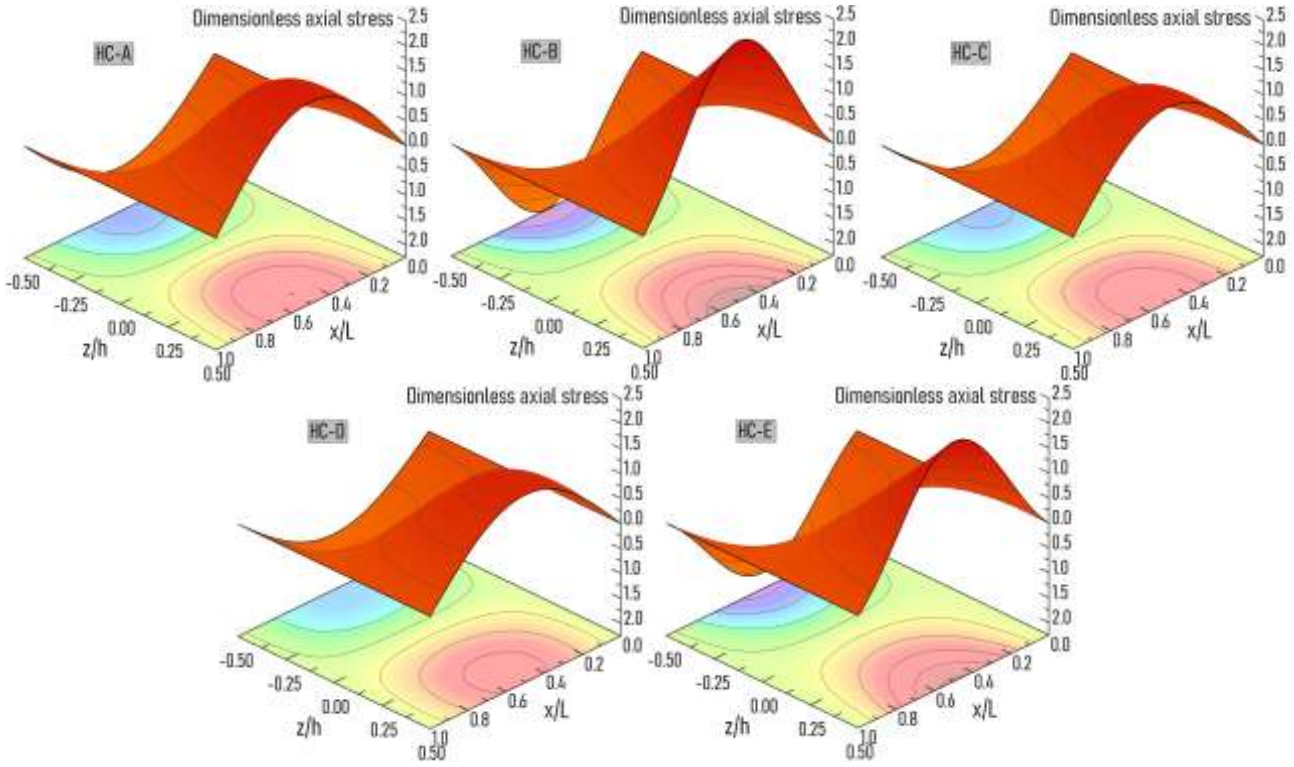

Fig. 9 Dimensionless axial stress "$\bar{\sigma}_{xx}$" distribution of various HC porous spherical shell patterns (SSSS, $e_0 = 0.3$, $a = b = 10h$)

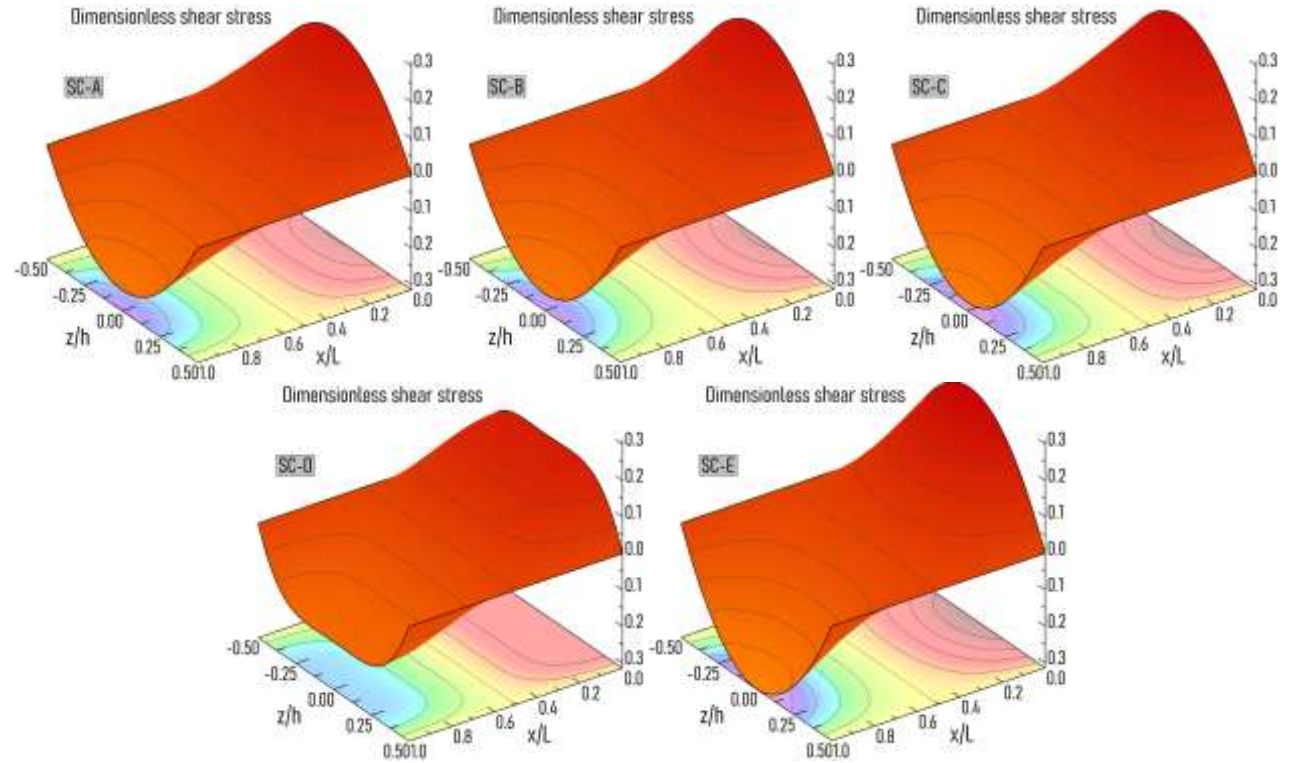

Fig. 10 Dimensionless shear stress "$\bar{\tau}_{xz}$" distribution of various SC porous spherical shell patterns (SSSS, $e_0 = 0.3$, $a = b = 10h$)

6.1 Effect of porosity distribution:

Fig. 5 shows the dimensionless central deflection as a function of the porosity coefficient e_0 for various porous spherical shell patterns. It is observed that an increase in the porosity coefficient reduces shell stiffness, leading to an increase in central deflection across all porosity distribution patterns. The effect of e_0 is notably more pronounced in

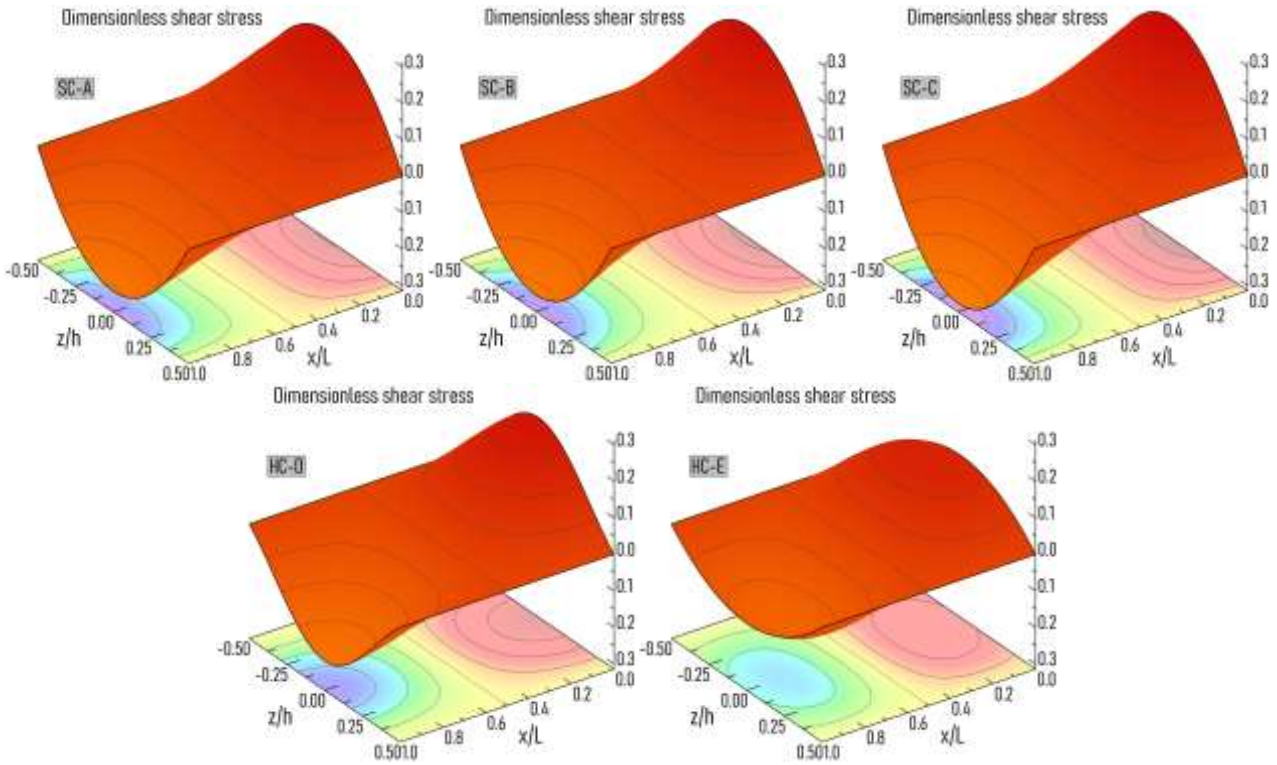

Fig. 11 Dimensionless shear stress "$\bar{\tau}_{xz}$" distribution of various HC porous spherical shell patterns (SSSS, $e_0 = 0.3$, $a = b = 10h$)

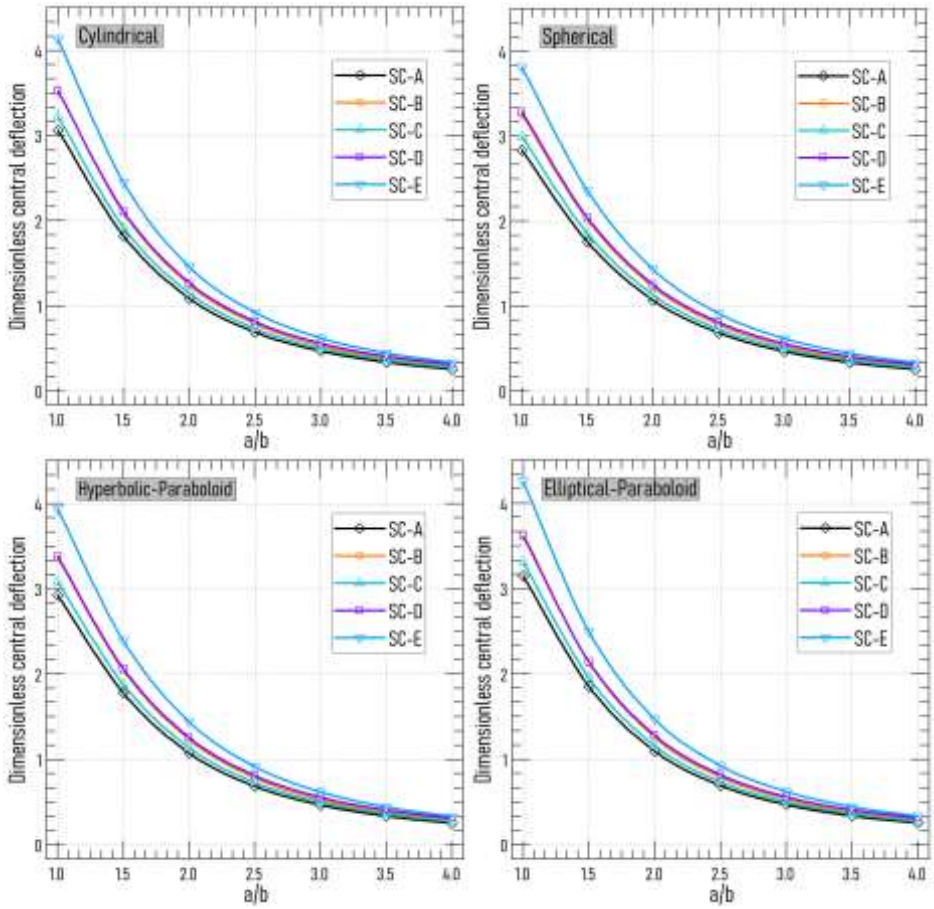

Fig. 12 Dimensionless central deflection "$\overline{w}$" versus aspect ratio "a/b" for various SC porous spherical shell patterns (SSSS, $e_0 = 0.3$, $a = b = 10h$)

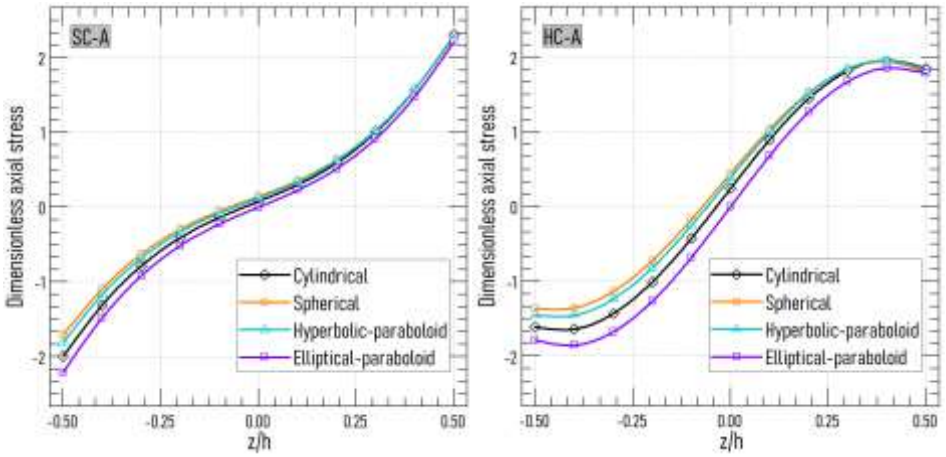

Fig. 13 Dimensionless shear stress "$\bar{\sigma}_{xx}$" of various schemes of 3D porous shells (SSSS, $e_0 = 0.3,\ a = b = 10h$)

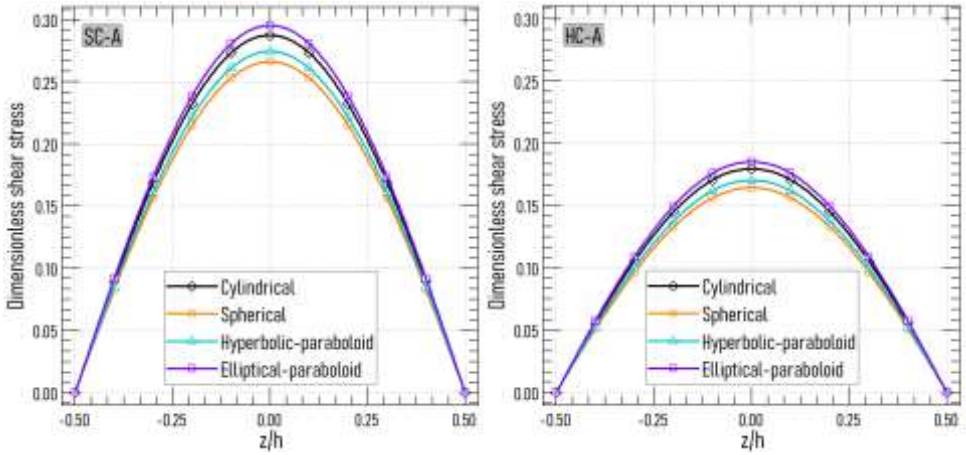

Fig. 14 Dimensionless shear stress "$\bar{\tau}_{xz}$" of various schemes of 3D porous shells (SSSS, $e_0 = 0.3,\ a = b = 10h$)

HC-E shells compared to SC-A shells. Fig. 6 plots the distribution of axial stresses for different values of the porosity coefficient e_0. A nearly linear variation of axial stress is observed for SC-A shells when e_0=0.2. The maximum stresses are consistently located at the top part of the shell, irrespective of the SC distribution patterns and inhomogeneity parameters. In contrast, the location of maximum stress values varies significantly in HC shells.

Fig. 7 illustrates the effect of the porosity coefficient e_0 on the dimensionless shear stress for 3D porous spherical shells. Increasing e_0 for SC-A shells results in higher shear stress values, while HC-A shells exhibit the opposite behavior. Figs. 8 and 9 present the distribution of dimensionless axial stress for different square simply supported porous spherical shell patterns, with e_0=0.3. These distributions show tensile stresses at the top surface and compressive stresses at the bottom surface, with stress values being zero at the edges (x=0,L). In SC porous shells, maximum stress values occur at the top and bottom surfaces, regardless of the distribution patterns. Figs. 10 and 11 depict the distribution of dimensionless axial stress for different square simply supported SC and HC porous spherical shell patterns. It is observed that the maximum shear stress values occur at the mid-plane of the shells, irrespective of the shell type.

6.2 Effect of shell geometry:

Fig. 12 presents the dimensionless central deflection as a function of the aspect ratio (a/b) for various SC porous spherical shell patterns. For all shell configurations and distribution patterns, an increase in the aspect ratio results in a reduction in dimensionless central deflection. The differences between results are more pronounced at lower aspect ratios. Fig. 13 shows the dimensionless shear stress for different 3D porous shell configurations. It is observed that the differences in stresses are particularly significant at the bottom of the shell, where compressive stresses are dominant. Fig. 14 illustrates the dimensionless shear stress) for various 3D porous shell patterns. The SC-A shell exhibits higher shear stresses compared to the HC-A shell. Among the different shell geometries, the Elliptical-paraboloid shells display the highest stress levels, while the spherical shells exhibit the lowest values.

7. Conclusions

This article investigates the deflection and stresses in a 3D functionally graded porous shell. The analytical solution is based on the generalized higher-order theory. Equilibrium

equations are derived using the virtual work principle and solved using the Galerkin method. The key findings, based on numerical calculations, are summarized as follows:

• An increase in the porosity coefficient decreases the stiffness of both hardcore and softcore porous shells, regardless of the distribution type, resulting in an increase in deflection.

• The stiffest shells are the hardcore SC-A shell and the softcore HC-E shell.

• Increasing the thickness ratio leads to a reduction in central deflections, regardless of the shell type.

• For all shell configurations and distribution patterns, increasing the aspect ratio reduces the dimensionless central deflection, with the variations being more noticeable at lower aspect ratios.

• In softcore SC shells, the maximum axial stresses occur at the top and bottom surfaces, with tensile stresses at the top and compressive stresses at the bottom.

• In hardcore shells, the maximum axial stresses are found inside the shell for FG-A, FG-C, and FG-D distributions, while for FG-B and FG-E distributions, they are located at the top and bottom surfaces.

• The maximum shear stresses occur at a point on the mid-plane of the shells, independent of shell type.

Acknowledgements

The authors gratefully acknowledge the funding of the Deanship Graduate Studies and Scientic Research, Jazan University, Saudi Arabia, through project number RG24-M029.

References

Abdelhaffez, G.S., Daikh, A.A., Saleem, H.A. and Eltaher, M.A. (2023), "Buckling of coated functionally graded spherical nanoshells resting on an orthotropic elastic medium", *Mathematics*, **11**(2), 409. https://doi.org/10.3390/math11020409

Abouelregal, A.E., Mohammed, W.W. and Mohammad-Sedighi, H. (2021), "Vibration analysis of functionally graded microbeam under initial stress via a generalized thermoelastic model with dual-phase lags", *Arch. Appl. Mech.*, **91**, 2127-2142. https://doi.org/10.1007/s00419-020-01873-2

Ahmadi, H. and Foroutan, K. (2020), "Nonlinear static and dynamic thermal buckling analysis of imperfect multilayer functionally graded cylindrical shells with a porous core on a nonlinear elastic foundation", *J. Therm. Stress.*, **43**(5), 629-649. https://doi.org/10.1080/01495739.2020.1727802

Artioli, E. and Viola, E. (2005), "Static analysis of shear-deformable shells of revolution using the generalized differential quadrature method", *Struct. Eng. Mech.*, **19**(4), 459. https://doi.org/10.12989/sem.2005.19.4.459

Asadi, E. and Qatu, M.S. (2012), "Static analysis of thick laminated shells with varying boundary conditions using the generalized differential quadrature method", *Thin Wall. Struct.*, **51**, 76-81. https://doi.org/10.1016/j.tws.2011.11.004

Banhart, J. (2001), "Manufacture, characterization, and application of cellular metals and metal foams", *Prog. Mater. Sci.*, **46**(6), 559-632. https://doi.org/10.1016/S0079-6425(00)00002-5

Barbero, E.J., Madeo, A., Zagari, G., Zinno, R. and Zucco, G. (2014), "A mixed isostatic 24 DOF element for static and buckling analysis of laminated folded plates", *Compos. Struct.*, **116**, 223-234. http://doi.org/10.1016/j.compstruct.2014.05.003

Belarbi, M.O., Houari, M.S.A., Daikh, A.A., Garg, A., Merzouki, T., Chalak, H.D. and Hirane, H. (2021), "Nonlocal finite element model for the bending and buckling analysis of functionally graded nanobeams using a novel shear deformation theory", *Compos. Struct.*, **264**, 113712. https://doi.org/10.1016/j.compstruct.2021.113712

Carrera, E., Zappino, E. and Cavallo, T. (2016), "Static analysis of reinforced thin-walled plates and shells using finite element models", *Int. J. Comput. Meth. Eng. Sci. Mech.*, **17**(2), 106-126. http://doi.org/10.1080/15502287.2016.1157647

Chai, Y., Li, W., Liu, G., Gong, Z. and Li, T. (2017), "A super-convergent alpha finite element method (SαFEM) for the static and free vibration analysis of shell structures", *Comput. Struct.*, **179**, 27-47. http://dx.doi.org/10.1016/j.compstruc.2016.10.021

Chau-Dinh, T. (2023), "Analysis of shell structures using an improved 3-node triangular flat shell element with a bubble function and cell-based strain smoothing", *Thin Wall. Struct.*, **182**, 110222. https://doi.org/10.1016/j.tws.2022.110222

Clausen, A., Andreassen, E. and Sigmund, O. (2017), "Topology optimization of 3D shell structures with porous infill", *Acta Mechanica Sinica*, **33**, 778-791. https://doi.org/10.1007/s10409-017-0679-2

Daikh, A.A., Hamdi, A., Ahmed, H.M., Abdelwahed, M.S., Abdelrahman, A.A. and Eltaher, M.A. (2023), "Buckling and bending of coated functionally graded graphene-reinforced composite plates and shells", *Adv. Nano Res.*, **15**(2), 113-128. https://doi.org/10.12989/anr.2023.15.2.113

Dang, V.H., Sedighi, H.M., Chan, D.Q., Civalek, O. and Abouelregal, A.E. (2021), "Nonlinear vibration and stability of FG nanotubes conveying fluid via nonlocal strain gradient theory", *Struct. Eng. Mech.*, **78**(1), 103-116. https://doi.org/10.12989/sem.2021.78.1.103

Ding, H.X. and She, G.L. (2024), "Nonlinear combined resonances of axially moving graphene platelets reinforced metal foam cylindrical shells under forced vibrations", *Nonlinear Dyn.*, **112**(1), 419-441. https://doi.org/10.1007/s11071-023-09059-5

Do, V.D., Le Grognec, P. and Rohart, P. (2023), "Closed-form solutions for the elastic–plastic buckling design of shell structures under external pressure", *Eur. J. Mech. A Solids*, **98**, 104861. https://doi.org/10.1016/j.euromechsol.2022.104861

Fu, T., Hu, X. and Yang, C. (2023), "Impact response analysis of stiffened sandwich functionally graded porous materials doubly-curved shells with a re-entrant honeycomb auxetic core", *Appl. Math. Modell.*, **124**, 553-575. https://doi.org/10.1016/j.apm.2023.08.024

Garg, A., Belarbi, M.O., Chalak, H.D. and Chakrabarti, A. (2021), "A review of the analysis of sandwich FGM structures", *Compos. Struct.*, **258**, 113427. https://doi.org/10.1016/j.compstruct.2020.113427

Garg, A., Belarbi, M.O., Li, L. and Tounsi, A. (2022), "Bending analysis of power-law sandwich FGM beams under thermal conditions", *Adv. Aircr. Spacecr. Sci.*, **9**(3), 243-261. https://doi.org/10.12989/aas.2022.9.3.243

Garg, A., Belarbi, M.O., Li, L., Chalak, H.D. and Tounsi, A. (2023), "Comparative study on the bending of exponential and sigmoidal sandwich beams under thermal conditions", *Struct. Eng. Mech.*, **85**(2), 217-231. https://doi.org/10.12989/sem.2023.85.2.217

Garg, A., Belarbi, M.O., Tounsi, A., Li, L., Singh, A. and Mukhopadhyay, T. (2022), "Predicting elemental stiffness matrix of FG nanoplates using Gaussian Process Regression based surrogate model in framework of layerwise model", *Eng. Anal. Bound. Elem.*, **143**, 779-795.

https://doi.org/10.1016/j.enganabound.2022.08.001

Garg, A., Chalak, H.D., Zenkour, A.M., Belarbi, M.O. and Houari, M.S.A. (2022), "A review of available theories and methodologies for the analysis of nano isotropic, nano functionally graded, and CNT reinforced nanocomposite structures", *Arch. Comput. Meth. Eng.*, **29**, 2237-2270. https://doi.org/10.1007/s11831-021-09652-0

Garg, A., Gupta, S., Chalak, H.D., Belarbi, M.O., Tounsi, A., Li, L. and Zenkour, A.M. (2023), "Free vibration analysis of power-law and sigmoidal sandwich FG plates using refined zigzag theory", *Adv. Mater. Res.*, **12**(1), 43-65. https://doi.org/10.12989/amr.2023.12.1.043

Garg, A., Mukhopadhyay, T., Chalak, H.D., Belarbi, M.O., Li, L. and Sahoo, R. (2022), "Multiscale bending and free vibration analyses of functionally graded graphene platelet/fiber composite beams", *Steel Compos. Struct.*, **44**(5), 707-720. https://doi.org/10.12989/scs.2022.44.5.707

Ghalambaz, M., Aljaghtham, M., Chamkha, A.J., Fteiti, M. and Abdullah, A. (2023), "Latent heat thermal energy storage in a shell-tube: A wavy partial layer of metal foam over tubes", *J. Energy Storage*, **59**, 106493. https://doi.org/10.1016/j.est.2022.106493

Ghandourah, E.E., Daikh, A.A., Khatir, S., Alhawsawi, A.M., Banoqitah, E.M. and Eltaher, M.A. (2023), "A dynamic analysis of porous coated functionally graded nanoshells resting on a viscoelastic medium", *Mathematics*, **11**(10), 2407. https://doi.org/10.3390/math11102407

Hadji, L., Plevris, V. and Papazafeiropoulos, G. (2024), "Investigation of the static bending response of FGM sandwich plates", *J. Appl. Comput. Mech.*, **10**(1), 26-37. https://doi.org/10.22055/jacm.2023.44278.4194

Hente, C., Gebhardt, C.G. and Rolfes, R. (2021), "On the static analysis of nonlinear beam and shell structures with singular stiffness matrices due to redundant coordinates", *Thin Wall. Struct.*, **161**, 107496. https://doi.org/10.1016/j.tws.2021.107496

Hieu, D.V., Chan, D.Q. and Sedighi, H.M. (2021), "Nonlinear bending, buckling and vibration of functionally graded nonlocal strain gradient nanobeams resting on an elastic foundation", *J. Mech. Mater. Struct.*, **16**(3), 327-346. https://doi.org/10.2140/jomms.2021.16.327

Houari, M.S.A., Bessaim, A., Merzouki, T., Daikh, A.A., Garg, A., Tounsi, A., Eltaher, M.A. and Belarbi, M.O. (2024), "Shear correction factors for a new exponential functionally graded porous beam", *Struct. Eng. Mech.*, **89**(1), 1-11. https://doi.org/10.12989/sem.2024.89.1.001

Hutchinson, J.W. and He, M.Y. (2000), "Buckling of cylindrical sandwich shells with metal foam cores", *Int. J. Solids Struct.*, **37**(46-47), 6777-6794. https://doi.org/10.1016/S0020-7683(99)00314-5

Jena, S.K., Chakraverty, S., Mahesh, V., Harursampath, D. and Sedighi, H.M. (2022), "Free vibration of functionally graded beam embedded in Winkler-Pasternak elastic foundation with geometrical uncertainties using symmetric Gaussian fuzzy number", *Eur. Phys. J. Plus*, **137**(3), 399. https://doi.org/10.1140/epjp/s13360-022-02607-9

Keleshteri, M.M. and Jelovica, J.J.E.S. (2022), "Analytical solution for vibration and buckling of cylindrical sandwich panels with improved FG metal foam core", *Eng. Struct.*, **266**, 114580. https://doi.org/10.1016/j.engstruct.2022.114580

Khaniki, H.B. and Ghayesh, M.H. (2023), "Highly nonlinear hyperelastic shells: Statics and dynamics", *Int. J. Eng. Sci.*, **183**, 103794. https://doi.org/10.1016/j.ijengsci.2022.103794

Ladmek, M., Belkacem, A., Daikh, A.A., Bessaim, A., Garg, A., Houari, M.S.A., Belarbi, M.O. and Ouldyerou, A. (2023), "Free vibration of functionally graded carbon nanotubes reinforced composite nanobeams", *Adv. Mater. Res.*, **12**(2), 161-177. https://doi.org/10.12989/amr.2023.12.2.161

Li, H., Hao, Y.X., Zhang, W., Liu, L.T., Yang, S.W. and Wang, D.M. (2021), "Vibration analysis of porous metal foam truncated conical shells with general boundary conditions using GDQ", *Compos. Struct.*, **269**, 114036. https://doi.org/10.1016/j.compstruct.2021.114036

Li, S., Wang, Z., Wu, G., Zhao, L. and Li, X. (2014), "Dynamic response of sandwich spherical shells with graded metallic foam cores subjected to blast loading", *Compos. Part A Appl. Sci. Manuf.*, **56**, 262-271. http://doi.org/10.1016/j.compositesa.2013.10.019

Liu, L., Liu, G.R. and Tan, V.B. (2002), "Element-free method for static and free vibration analysis of spatial thin shell structures", *Comput. Meth. Appl. Mech. Eng.*, **191**(51-52), 5923-5942. https://doi.org/10.1016/S0045-7825(02)00504-2

Medjdoubi, B.A., Houari, M.S.A., Sadoun, M., Bessaim, A., Daikh, A.A., Belarbi, M.O., Khechai, A., Garg, A. and Ghazwani, M.H. (2023), "On the effect of porosity on the shear correction factors of functionally graded porous beams", *Coupled Syst. Mech.*, **12**(3), 199-220. https://doi.org/10.12989/csm.2023.12.3.199

Melaibari, A., Daikh, A.A., Basha, M., Abdalla, A.W., Othman, R., Almitani, K.H., Hamed, M.A., Abdelrahman, A. and Eltaher, M.A. (2022b), "Free vibration of FG-CNTRCs nano-plates/shells with temperature-dependent properties", *Mathematics*, **10**, 583. https://doi.org/10.3390/math10040583

Melaibari, A., Daikh, A.A., Basha, M., Wagih, A., Othman, R., Almitani, K.H., Hamed, M.A., Abdelrahman, A. and Eltaher, M.A. (2022a), "A dynamic analysis of randomly oriented functionally graded carbon nanotubes/fiber-reinforced composite laminated shells with different geometries", *Mathematics*, **10**(3), 408. https://doi.org/10.3390/math10030408

Pinho, F.A.X.C., Del Prado, Z.J.G.N. and da Silva, F.M.A. (2022), "Nonlinear static analysis of thin shallow and non-shallow shells using tensor formulation", *Eng. Struct.*, **253**, 113674. https://doi.org/10.1016/j.engstruct.2021.113674

Punera, D. and Kant, T. (2019), "A critical review of stress and vibration analyses of functionally graded shell structures", *Compos. Struct.*, **210**, 787-809. https://doi.org/10.1016/j.compstruct.2018.11.084

Radwańska, M., Stankiewicz, A., Wosatko, A. and Pamin, J. (2017), "Plate and shell structures: Selected analytical and finite element solutions", John Wiley & Sons.

Ramteke, P.M. and Panda, S.K. (2023), "Nonlinear static and dynamic response prediction of bidirectional doubly-curved porous FG panel and experimental validation", *Compos. Part A Appl. Sci. Manuf.*, **166**, 107388. https://doi.org/10.1016/j.compositesa.2022.107388

Rizov, V. (2024), "The effect of delamination between layers in U-shaped members made of functionally graded multilayered viscoelastic materials", *J. Appl. Comput. Mech.*, **10**(4), 830-841. https://doi.org/10.22055/jacm.2024.46014.4449

Sedighi, H.M. and Malikan, M. (2020), "Stress-driven nonlocal elasticity for nonlinear vibration characteristics of carbon/ boron-nitride hetero-nanotube subject to magneto-thermal environment", *Physica Scripta*, **95**(5), 055218. https://doi.org/10.1088/1402-4896/ab7a38

Sedighi, H.M., Ouakad, H.M., Dimitri, R. and Tornabene, F. (2020), "Stress-driven nonlocal elasticity for the instability analysis of fluid-conveying C-BN hybrid-nanotube in a magneto-thermal environment", *Physica Scripta*, **95**(6), 065204. https://doi.org/10.1088/1402-4896/ab793f

Shariati, A., Jung, D.W., Mohammad-Sedighi, H., Żur, K.K., Habibi, M. and Safa, M. (2020), "On the vibrations and stability of moving viscoelastic axially functionally graded nanobeams", *Materials*, **13**(7), 1707. https://doi.org/10.3390/ma13071707

Sobhy, M. and Radwan, A.F. (2023), "Porosity and size effects on electro-hygrothermal bending of FG sandwich piezoelectric cylindrical shells with porous core via a four-variable shell theory", *Case Stud. Therm. Eng.*, **45**, 102934. https://doi.org/10.1016/j.csite.2023.102934

Son, L.T., Vinh, P.V., Chinh, N.V. and M. Sedighi, H. (2024), "High-frequency temperature-dependent vibration of nonlocal functionally graded sandwich nanoplates resting on elastic foundations", *Mech. Adv. Mater. Struct.*, 1-22. https://doi.org/10.1080/15376494.2024.2358108

Song, J.P. and She, G.L. (2024), "Nonlinear resonance and chaotic dynamics of rotating graphene platelets reinforced metal foam plates in a thermal environment", *Arch. Civil Mech. Eng.*, **24**(1), 1-31. https://doi.org/10.1007/s43452-023-00846-w

Tharwan, M.Y., Daikh, A.A., Assie, A.E., Alnujaie, A. and Eltaher, M.A. (2023), "A comprehensive study on the static response of agglomerated microstructure-dependent coated functionally graded carbon nanotubes reinforced composite nanoshells resting on a complex elastic foundation", *Mech. Based Des. Struct.*, 1-41. https://doi.org/10.1080/15397734.2023.2286484

Toan Thang, P., Nguyen-Thoi, T. and Lee, J. (2020), "Mechanical stability of metal foam cylindrical shells with various porosity distributions", *Mech. Adv. Mater. Struct.*, **27**(4), 295-303. https://doi.org/10.1080/15376494.2018.1472338

Tornabene, F., Viscoti, M. and Dimitri, R. (2023), "Static analysis of anisotropic doubly-curved shells subjected to concentrated loads employing higher-order layer-wise theories", *Comput. Model. Eng. Sci.*, **134**(2), 1393-468.

Viola, E., Tornabene, F. and Fantuzzi, N. (2013), "Static analysis of completely doubly-curved laminated shells and panels using general higher-order shear deformation theories", *Compos. Struct.*, **101**, 59-93. http://doi.org/10.1016/j.compstruct.2013.01.002

Wang, Y.Q., Ye, C. and Zu, J.W. (2019), "Vibration analysis of circular cylindrical shells made of metal foams under various boundary conditions", *Int. J. Mech. Mater. Des.*, **15**, 333-344. https://doi.org/10.1007/s10999-018-9415-8

Xin, L. and Kiani, Y. (2023), "Vibration characteristics of an arbitrary thick sandwich beam with a metal foam core resting on an elastic medium", *Structures*, **49**, 1-11. https://doi.org/10.1016/j.istruc.2023.01.108

Xue, Y., Jin, G., Zhang, C., Han, X. and Chen, J. (2023), "Free vibration analysis of functionally graded porous cylindrical panels and shells with porosity distributions along the thickness and length directions", *Thin Wall. Struct.*, **184**, 110448. https://doi.org/10.1016/j.tws.2022.110448

Zghal, S., Frikha, A. and Dammak, F. (2017), "Static analysis of functionally graded carbon nanotube-reinforced plate and shell structures", *Compos. Struct.*, 176, 1107-1123. http://doi.org/10.1016/j.compstruct.2017.06.015

Zhao, J., Xie, F., Wang, A., Shuai, C., Tang, J. and Wang, Q. (2019), "A unified solution for the vibration analysis of functionally graded porous (FGP) shallow shells with general boundary conditions", *Compos. Part B Eng.*, **156**, 406-424. https://doi.org/10.1016/j.compositesb.2018.08.115

CC

Appendix

$$K_{11} = A_{11}\int_0^a\int_0^b \frac{\partial^3 X_m}{\partial x^3} Y_n \frac{\partial X_m}{\partial x} Y_n \,\mathrm{d}x\mathrm{d}y +$$
$$A_{66}\int_0^a\int_0^b \frac{\partial X_m}{\partial x}\frac{\partial^2 Y_n}{\partial y^2}\frac{\partial X_m}{\partial x} Y_n \,\mathrm{d}x\mathrm{d}y - \boldsymbol{\lambda}\Big[(A_{11} +$$
$$A_{66})\int_0^a\int_0^b \frac{\partial^3 X_m}{\partial x^3}\frac{\partial^2 Y_n}{\partial y^2}\frac{\partial X_m}{\partial x} Y_n \,\mathrm{d}x\mathrm{d}y +$$
$$A_{11}\int_0^a\int_0^b \frac{\partial^5 X_m}{\partial x^5} Y_n \frac{\partial X_m}{\partial x} Y_n \,\mathrm{d}x\mathrm{d}y + A_{66}\int_0^a\int_0^b \frac{\partial X_m}{\partial x}\frac{\partial^4 Y_n}{\partial y^4}\frac{\partial X_m}{\partial x} Y_n \,\mathrm{d}x\mathrm{d}y\Big]$$
$$K_{12} = (A_{12} + A_{66})\Big(\int_0^a\int_0^b \frac{\partial X_m}{\partial x}\frac{\partial^2 Y_n}{\partial y^2}\frac{\partial X_m}{\partial x} Y_n \,\mathrm{d}x\mathrm{d}y -$$
$$\boldsymbol{\lambda}\Big[\int_0^a\int_0^b \frac{\partial^3 X_m}{\partial x^3}\frac{\partial^2 Y_n}{\partial y^2}\frac{\partial X_m}{\partial x} Y_n \,\mathrm{d}x\mathrm{d}y + \int_0^a\int_0^b \frac{\partial X_m}{\partial x}\frac{\partial^4 Y_n}{\partial y^4}\frac{\partial X_m}{\partial x} Y_n \,\mathrm{d}x\mathrm{d}y\Big]\Big)$$
$$K_{13} = \Big(\frac{A_{11}}{R_x} + \frac{A_{12}}{R_y}\Big)\Big(\int_0^a\int_0^b \frac{\partial X_m}{\partial x} Y_n \frac{\partial X_m}{\partial x} Y_n \,\mathrm{d}x\mathrm{d}y -$$
$$\lambda\Big[\int_0^a\int_0^b \frac{\partial^3 X_m}{\partial x^3} Y_n \frac{\partial X_m}{\partial x} Y_n \,\mathrm{d}x\mathrm{d}y + \int_0^a\int_0^b \frac{\partial X_m}{\partial x}\frac{\partial^2 Y_n}{\partial y^2}\frac{\partial X_m}{\partial x} Y_n \,\mathrm{d}x\mathrm{d}y\Big]\Big) -$$
$$B_{11}\int_0^a\int_0^b \frac{\partial^3 X_m}{\partial x^3} Y_n \frac{\partial X_m}{\partial x} Y_n \,\mathrm{d}x\mathrm{d}y - (B_{12} +$$
$$2B_{66})\int_0^a\int_0^b \frac{\partial X_m}{\partial x}\frac{\partial^2 Y_n}{\partial y^2}\frac{\partial X_m}{\partial x} Y_n \,\mathrm{d}x\mathrm{d}y - \boldsymbol{\lambda}\Big[-(B_{12} + 2B_{66} +$$
$$B_{11})\int_0^a\int_0^b \frac{\partial^3 X_m}{\partial x^3}\frac{\partial^2 Y_n}{\partial y^2}\frac{\partial X_m}{\partial x} Y_n \,\mathrm{d}x\mathrm{d}y -$$
$$B_{11}\int_0^a\int_0^b \frac{\partial^5 X_m}{\partial x^5} Y_n \frac{\partial X_m}{\partial x} Y_n \,\mathrm{d}x\mathrm{d}y\Big]$$
$$K_{14} = -C_{11}\int_0^a\int_0^b \frac{\partial^3 X_m}{\partial x^3} Y_n \frac{\partial X_m}{\partial x} Y_n \,\mathrm{d}x\mathrm{d}y - (C_{12} +$$
$$2C_{66})\int_0^a\int_0^b \frac{\partial X_m}{\partial x}\frac{\partial^2 Y_n}{\partial y^2}\frac{\partial X_m}{\partial x} Y_n \,\mathrm{d}x\mathrm{d}y - \boldsymbol{\lambda}\Big[-(B_{12} + 2B_{66} +$$
$$B_{11})\int_0^a\int_0^b \frac{\partial^3 X_m}{\partial x^3}\frac{\partial^2 Y_n}{\partial y^2}\frac{\partial X_m}{\partial x} Y_n \,\mathrm{d}x\mathrm{d}y -$$
$$B_{11}\int_0^a\int_0^b \frac{\partial^5 X_m}{\partial x^5} Y_n \frac{\partial X_m}{\partial x} Y_n \,\mathrm{d}x\mathrm{d}y\Big]$$
$$K_{21} = (A_{12} + A_{66})\Big(\int_0^a\int_0^b \frac{\partial^2 X_m}{\partial x^1}\frac{\partial Y_n}{\partial y} X_m \frac{\partial Y_n}{\partial y}\mathrm{d}x\mathrm{d}y -$$
$$\boldsymbol{\lambda}\Big[\int_0^a\int_0^b \frac{\partial^4 X_m}{\partial x^4}\frac{\partial Y_n}{\partial y} X_m \frac{\partial Y_n}{\partial y}\mathrm{d}x\mathrm{d}y + \int_0^a\int_0^b \frac{\partial^2 X_m}{\partial x^2}\frac{\partial^3 Y_n}{\partial y^3} X_m \frac{\partial Y_n}{\partial y}\mathrm{d}x\mathrm{d}y\Big]\Big)$$
$$K_{22} = A_{22}\int_0^a\int_0^b X_m \frac{\partial^3 Y_n}{\partial y^3} X_m \frac{\partial Y_n}{\partial y}\mathrm{d}x\mathrm{d}y +$$
$$A_{66}\int_0^a\int_0^b\int_0^b \frac{\partial^2 X_m}{\partial x^2}\frac{\partial Y_n}{\partial y} X_m \frac{\partial Y_n}{\partial y}\mathrm{d}x\mathrm{d}y - \boldsymbol{\lambda}\Big[(A_{22} +$$
$$A_{66})\int_0^a\int_0^b \frac{\partial^2 X_m}{\partial x^2}\frac{\partial^3 Y_n}{\partial y^3} X_m \frac{\partial Y_n}{\partial y}\mathrm{d}x\mathrm{d}y +$$
$$A_{22}\int_0^a\int_0^b X_m \frac{\partial^5 Y_n}{\partial y^5} X_m \frac{\partial Y_n}{\partial y}\mathrm{d}x\mathrm{d}y + A_{66}\int_0^a \frac{\partial^4 X_m}{\partial x^4}\frac{\partial Y_n}{\partial y} X_m \frac{\partial Y_n}{\partial y}\mathrm{d}x\mathrm{d}y\Big]$$
$$K_{23} = \Big(\frac{A_{12}}{R_x} + \frac{A_{22}}{R_y}\Big)\Big(\int_0^a\int_0^b X_m \frac{\partial Y_n}{\partial y} X_m \frac{\partial Y_n}{\partial y}\mathrm{d}x\mathrm{d}y -$$
$$\lambda\Big[\int_0^a\int_0^b \frac{\partial^2 X_m}{\partial x^2}\frac{\partial Y_n}{\partial y} X_m \frac{\partial Y_n}{\partial y}\mathrm{d}x\mathrm{d}y + \int_0^a\int_0^b X_m \frac{\partial^3 Y_n}{\partial y^3} X_m \frac{\partial Y_n}{\partial y}\mathrm{d}x\mathrm{d}y\Big]\Big) -$$
$$B_{22}\int_0^a\int_0^b X_m \frac{\partial^3 Y_n}{\partial y^3} X_m \frac{\partial Y_n}{\partial y}\mathrm{d}x\mathrm{d}y - (B_{12} +$$
$$2B_{66})\int_0^a\int_0^b \frac{\partial X_m}{\partial x}\frac{\partial^2 Y_n}{\partial y^2} X_m \frac{\partial Y_n}{\partial y}\mathrm{d}x\mathrm{d}y -$$
$$-\lambda\Big[-B_{22}\Big(\int_0^a\int_0^b \frac{\partial^2 X_m}{\partial x^2}\frac{\partial^3 Y_n}{\partial y^3} X_m \frac{\partial Y_n}{\partial y}\mathrm{d}x\mathrm{d}y + \int_0^a\int_0^b X_m \frac{\partial^5 Y_n}{\partial y^5} X_m \frac{\partial Y_n}{\partial y}\mathrm{d}x\mathrm{d}y\Big) -$$
$$(B_{12} + 2B_{66})\Big(\int_0^a\int_0^b \frac{\partial^3 X_m}{\partial x^3}\frac{\partial^2 Y_n}{\partial y^2} X_m \frac{\partial Y_n}{\partial y}\mathrm{d}x\mathrm{d}y +$$
$$\int_0^a\int_0^b \frac{\partial X_m}{\partial x}\frac{\partial^4 Y_n}{\partial y^4} X_m \frac{\partial Y_n}{\partial y}\mathrm{d}x\mathrm{d}y\Big)\Big]$$
$$K_{24} = -C_{22}\int_0^a\int_0^b X_m \frac{\partial^3 Y_n}{\partial y^3} X_m \frac{\partial Y_n}{\partial y}\mathrm{d}x\mathrm{d}y - (C_{12} +$$
$$2C_{66})\int_0^a\int_0^b \frac{\partial^2 X_m}{\partial x^2}\frac{\partial Y_n}{\partial y} X_m \frac{\partial Y_n}{\partial y}\mathrm{d}x\mathrm{d}y -$$
$$\lambda\Big[-C_{22}\Big(\int_0^a\int_0^b \frac{\partial^2 X_m}{\partial x^2}\frac{\partial^3 Y_n}{\partial y^3} X_m \frac{\partial Y_n}{\partial y}\mathrm{d}x\mathrm{d}y +$$
$$\int_0^a\int_0^b X_m \frac{\partial^5 Y_n}{\partial y^5} X_m \frac{\partial Y_n}{\partial y}\mathrm{d}x\mathrm{d}y\Big) - (C_{12} +$$
$$2C_{66})\Big(\int_0^a\int_0^b \frac{\partial^4 X_m}{\partial x^4}\frac{\partial Y_n}{\partial y} X_m \frac{\partial Y_n}{\partial y}\mathrm{d}x\mathrm{d}y +$$
$$\int_0^a\int_0^b \frac{\partial^2 X_m}{\partial x^2}\frac{\partial^3 Y_n}{\partial y^3} X_m \frac{\partial Y_n}{\partial y}\mathrm{d}x\mathrm{d}y\Big)\Big]$$
$$K_{31} = -\Big(\frac{A_{11}}{R_x} + \frac{A_{12}}{R_y}\Big)\Big(\int_0^a\int_0^b \frac{\partial^2 X_n}{\partial x^2} Y_n X_m Y_n \,\mathrm{d}x\mathrm{d}y -$$
$$\lambda\Big[\int_0^a\int_0^b \frac{\partial^4 X_n}{\partial x^4} Y_n X_m Y_n \,\mathrm{d}x\mathrm{d}y + \int_0^a\int_0^b \frac{\partial^2 X_n}{\partial x^2}\frac{\partial^2 Y_n}{\partial y^2} X_m Y_n \,\mathrm{d}x\mathrm{d}y\Big]\Big) +$$
$$B_{11}\int_0^a\int_0^b \frac{\partial^4 X_n}{\partial x^4} Y_n X_m Y_n \,\mathrm{d}x\mathrm{d}y + (B_{12} +$$
$$2B_{66})\int_0^a\int_0^b \frac{\partial^2 X_m}{\partial x^2}\frac{\partial^2 Y_n}{\partial y^2} X_m Y_n \,\mathrm{d}x\mathrm{d}y -$$
$$\lambda\Big[B_{11}\int_0^a\int_0^b \frac{\partial^6 X_n}{\partial x^6} Y_n X_m Y_n \,\mathrm{d}x\mathrm{d}y + (B_{11} + B_{12} +$$
$$2B_{66})\int_0^a\int_0^b \frac{\partial^4 X_m}{\partial x^4}\frac{\partial^2 Y_n}{\partial y^2} X_m Y_n \,\mathrm{d}x\mathrm{d}y + (B_{12} +$$

$$2B_{66})\int_0^a\int_0^b \frac{\partial^2 X_m}{\partial x^2}\frac{\partial^4 Y_n}{\partial y^4}X_mY_n\,dxdy\Big]$$

$$K_{23}=-\left(\frac{A_{12}}{R_x}+\frac{A_{22}}{R_y}\right)\left(\int_0^a\int_0^b X_m\frac{\partial^2 Y_n}{\partial y^2}X_mY_n\,dxdy-\right.$$

$$\lambda\left[\int_0^a\int_0^b \frac{\partial^2 X_m}{\partial x^2}\frac{\partial^2 Y_n}{\partial y^2}X_mY_n\,dxdy+\int_0^a\int_0^b X_m\frac{\partial^4 Y_n}{\partial y^4}X_mY_n\,dxdy\right]\Big)+$$

$$B_{22}\int_0^a\int_0^b X_m\frac{\partial^4 Y_n}{\partial y^4}X_mY_n\,dxdy+(B_{12}+$$

$$2B_{66})\int_0^a\int_0^b \frac{\partial^2 X_m}{\partial x^2}\frac{\partial^2 Y_n}{\partial y^2}X_mY_n\,dxdy-\lambda\Big[(B_{22}+B_{12}+$$

$$2B_{66})\int_0^a\int_0^b \frac{\partial^2 X_m}{\partial x^2}\frac{\partial^4 Y_n}{\partial y^4}X_mY_n\,dxdy+(B_{12}+$$

$$2B_{66})\int_0^a\int_0^b \frac{\partial^4 X_m}{\partial x^4}\frac{\partial^2 Y_n}{\partial y^2}X_mY_n\,dxdy+$$

$$B_{22}\int_0^a\int_0^b X_m\frac{\partial^6 Y_n}{\partial y^6}X_mY_n\,dxdy\Big]$$

$$K_{33}=2\left(\frac{B_{11}}{R_x}+\frac{B_{12}}{R_y}\right)\left(\int_0^a\int_0^b \frac{\partial^2 X_n}{\partial x^2}Y_nX_mY_n\,dxdy-\right.$$

$$\lambda\left[\int_0^a\int_0^b \frac{\partial^4 X_m}{\partial x^4}Y_nX_mY_n\,dxdy+\int_0^a\int_0^b \frac{\partial^2 X_n}{\partial x^2}\frac{\partial^2 Y_n}{\partial y^2}X_mY_n\,dxdy\right]\Big)+$$

$$2\left(\frac{B_{12}}{R_x}+\frac{B_{22}}{R_y}\right)\left(\int_0^a\int_0^b X_m\frac{\partial^2 Y_n}{\partial y^2}X_mY_n\,dxdy-\right.$$

$$\lambda\left[\int_0^a\int_0^b \frac{\partial^2 X_m}{\partial x^2}\frac{\partial^2 Y_n}{\partial y^2}X_mY_n\,dxdy+\int_0^a\int_0^b X_m\frac{\partial^4 Y_n}{\partial y^4}X_mY_n\,dxdy\right]\Big)-$$

$$\left(\frac{A_{11}}{{R_x}^2}+2\frac{A_{12}}{R_xR_y}+\frac{A_{22}}{{R_y}^2}\right)\left(\int_0^a\int_0^b X_mY_nX_mY_n\,dxdy-\right.$$

$$\lambda\left[\int_0^a\int_0^b \frac{\partial^2 X_m}{\partial x^2}Y_nX_mY_n\,dxdy+\int_0^a\int_0^b X_m\frac{\partial^2 Y_n}{\partial y^2}X_mY_n\,dxdy\right]\Big)-$$

$$D_{11}\int_0^a\int_0^b \frac{\partial^4 X_m}{\partial x^4}Y_nX_mY_n\,dxdy-$$

$$D_{22}\left(\int_0^a\int_0^b X_m\frac{\partial^4 Y_n}{\partial y^4}X_mY_n\,dxdy\right)-2(D_{12}+$$

$$2D_{66})\int_0^a\int_0^b \frac{\partial^2 X_m}{\partial x^2}\frac{\partial^2 Y_n}{\partial y^2}X_mY_n\,dxdy-$$

$$\lambda\Big[-D_{11}\int_0^a\int_0^b \frac{\partial^6 X_m}{\partial x^6}Y_nX_mY_n\,dxdy-$$

$$D_{22}\int_0^a\int_0^b X_m\frac{\partial^6 Y_n}{\partial y^6}X_mY_n\,dxdy-(D_{11}+2D_{12}+$$

$$4D_{66})\int_0^a\int_0^b \frac{\partial^4 X_m}{\partial x^4}\frac{\partial^2 Y_n}{\partial y^2}X_mY_n\,dxdy-(D_{22}+2D_{12}+$$

$$4D_{66})\int_0^a\int_0^b \frac{\partial^2 X_m}{\partial x^2}\frac{\partial^4 Y_n}{\partial y^4}X_mY_n\,dxdy\Big]$$

$$K_{34}=-\left(\frac{C_{11}}{R_x}+\frac{C_{12}}{R_y}\right)\left(\int_0^a\int_0^b \frac{\partial^2 X_n}{\partial x^2}Y_nX_mY_n\,dxdy-\right.$$

$$\lambda\left[\int_0^a\int_0^b \frac{\partial^4 X_m}{\partial x^4}Y_nX_mY_n\,dxdy+\int_0^a\int_0^b \frac{\partial^2 X_n}{\partial x^2}\frac{\partial^2 Y_n}{\partial y^2}X_mY_n\,dxdy\right]\Big)-$$

$$\left(\frac{C_{12}}{R_x}+\frac{C_{22}}{R_y}\right)\left(\int_0^a\int_0^b X_m\frac{\partial^2 Y_n}{\partial y^2}X_mY_n\,dxdy-\right.$$

$$\lambda\left[\int_0^a\int_0^b \frac{\partial^2 X_m}{\partial x^2}\frac{\partial^2 Y_n}{\partial y^2}X_mY_n\,dxdy+\int_0^a\int_0^b X_m\frac{\partial^4 Y_n}{\partial y^4}X_mY_n\,dxdy\right]\Big)-$$

$$E_{11}\int_0^a\int_0^b \frac{\partial^4 X_m}{\partial x^4}Y_nX_mY_n\,dxdy-E_{22}\left(\int_0^a\int_0^b X_m\frac{\partial^4 Y_n}{\partial y^4}X_mY_n\,dxdy\right)-$$

$$2(E_{12}+2E_{66})\int_0^a\int_0^b \frac{\partial^2 X_m}{\partial x^2}\frac{\partial^2 Y_n}{\partial y^2}X_mY_n\,dxdy-$$

$$\lambda\Big[-E_{11}\int_0^a\int_0^b \frac{\partial^6 X_m}{\partial x^6}Y_nX_mY_n\,dxdy-$$

$$E_{22}\int_0^a\int_0^b X_m\frac{\partial^6 Y_n}{\partial y^6}X_mY_n\,dxdy-(E_{11}+2E_{12}+$$

$$4E_{66})\int_0^a\int_0^b \frac{\partial^4 X_m}{\partial x^4}\frac{\partial^2 Y_n}{\partial y^2}X_mY_n\,dxdy-(E_{22}+2E_{12}+$$

$$4E_{66})\int_0^a\int_0^b \frac{\partial^2 X_m}{\partial x^2}\frac{\partial^4 Y_n}{\partial y^4}X_mY_n\,dxdy\Big]$$

$$K_{41}=C_{11}\int_0^a\int_0^b \frac{\partial^4 X_m}{\partial x^4}Y_nX_mY_n\,dxdy+(C_{12}+$$

$$2C_{66})\int_0^a\int_0^b \frac{\partial^2 X_m}{\partial x^2}\frac{\partial^2 Y_n}{\partial y^2}X_mY_n\,dxdy-$$

$$\lambda\Big[C_{11}\int_0^a\int_0^b \frac{\partial^6 X_m}{\partial x^6}Y_nX_mY_n\,dxdy+(C_{12}+$$

$$2C_{66})\int_0^a\int_0^b \frac{\partial^2 X_m}{\partial x^2}\frac{\partial^4 Y_n}{\partial y^4}X_mY_n\,dxdy+(C_{11}+C_{12}+$$

$$2C_{66})\left(\int_0^a\int_0^b \frac{\partial^4 X_m}{\partial x^4}\frac{\partial^2 Y_n}{\partial y^2}X_mY_n\,dxdy\right)\Big]$$

$$K_{42}=C_{22}\int_0^a\int_0^b X_m\frac{\partial^4 Y_n}{\partial y^4}X_mY_n\,dxdy+(C_{12}+$$

$$2C_{66})\int_0^a\int_0^b \frac{\partial^2 X_m}{\partial x^2}\frac{\partial^2 Y_n}{\partial y^2}X_mY_n\,dxdy-$$

$$\lambda\Big[C_{22}\int_0^a\int_0^b X_m\frac{\partial^6 Y_n}{\partial y^6}X_mY_n\,dxdy+(C_{12}+$$

$$2C_{66})\int_0^a\int_0^b \frac{\partial^4 X_m}{\partial x^4}\frac{\partial^2 Y_n}{\partial y^2}X_mY_n\,dxdy\,(C_{22}+C_{12}+$$

$$2C_{66})\int_0^a\int_0^b \frac{\partial^2 X_m}{\partial x^2}\frac{\partial^4 Y_n}{\partial y^4}X_mY_n\,dxdy\Big]$$

$$K_{43}=-\left(\frac{C_{11}}{R_x}+\frac{C_{12}}{R_y}\right)\left(\int_0^a\int_0^b \frac{\partial X_m}{\partial x}Y_n\frac{\partial X_m}{\partial x}Y_n\,dxdy-\right.$$

$$\lambda\left[\int_0^a\int_0^b \frac{\partial^3 X_m}{\partial x^3}Y_n\frac{\partial X_m}{\partial x}Y_n\,dxdy+\int_0^a\int_0^b \frac{\partial X_m}{\partial x}\frac{\partial^2 Y_n}{\partial y^2}\frac{\partial X_m}{\partial x}Y_n\,dxdy\right]\Big)-$$

$$\left(\frac{C_{12}}{R_x}+\frac{C_{22}}{R_y}\right)\left(\int_0^a\int_0^b X_m\frac{\partial Y_n}{\partial y}X_m\frac{\partial Y_n}{\partial y}dxdy-\right.$$

$$\lambda\left[\int_0^a\int_0^b \frac{\partial^2 X_m}{\partial x^2}\frac{\partial Y_n}{\partial y}X_m\frac{\partial Y_n}{\partial y}dxdy+\int_0^a\int_0^b X_m\frac{\partial^3 Y_n}{\partial y^3}X_m\frac{\partial Y_n}{\partial y}dxdy\right]\Big)-$$

$$E_{11}\int_0^a\int_0^b \frac{\partial^4 X_m}{\partial x^4}Y_nX_mY_n\,dxdy-E_{22}\left(\int_0^a\int_0^b X_m\frac{\partial^4 Y_n}{\partial y^4}X_mY_n\,dxdy\right)-$$

$$2(E_{12}+2E_{66})\int_0^a\int_0^b \frac{\partial^2 X_m}{\partial x^2}\frac{\partial^2 Y_n}{\partial y^2}X_mY_n\,dxdy-$$

$$\lambda\Big[-E_{11}\int_0^a\int_0^b \frac{\partial^6 X_m}{\partial x^6}Y_nX_mY_n\,dxdy-$$

$$E_{22}\int_0^a\int_0^b X_m\frac{\partial^6 Y_n}{\partial y^6}X_mY_n\,dxdy-(E_{11}+2E_{12}+$$

$$4E_{66})\int_0^a\int_0^b \frac{\partial^4 X_m}{\partial x^4}\frac{\partial^2 Y_n}{\partial y^2}X_mY_n\,dxdy-(E_{22}+2E_{12}+$$

$$4E_{66})\int_0^a\int_0^b \frac{\partial^2 X_m}{\partial x^2}\frac{\partial^4 Y_n}{\partial y^4}X_mY_n\,dxdy\Big]$$

$$K_{44}=-F_{11}\int_0^a\int_0^b \frac{\partial^4 X_m}{\partial x^4}Y_nX_mY_n\,dxdy-$$

$$F_{22}\left(\int_0^a\int_0^b X_m\frac{\partial^4 Y_n}{\partial y^4}X_mY_n\,dxdy\right)-2(F_{12}+$$

$$2F_{66})\int_0^a\int_0^b \frac{\partial^2 X_m}{\partial x^2}\frac{\partial^2 Y_n}{\partial y^2}X_mY_n\,dxdy+$$

$$J_{44}\int_0^a\int_0^b X_m\frac{\partial^2 Y_n}{\partial y^2}X_mY_n\,dxdy+J_{55}\int_0^a\int_0^b \frac{\partial^2 X_m}{\partial x^2}Y_nX_mY_n\,dxdy-$$

$$\lambda\Big[-F_{11}\int_0^a\int_0^b \frac{\partial^6 X_m}{\partial x^6}Y_nX_mY_n\,dxdy-$$

$$F_{22}\int_0^a\int_0^b X_m\frac{\partial^6 Y_n}{\partial y^6}X_mY_n\,dxdy-(F_{11}+2F_{12}+$$

$$4F_{66})\int_0^a\int_0^b \frac{\partial^4 X_m}{\partial x^4}\frac{\partial^2 Y_n}{\partial y^2}X_mY_n\,dxdy-(F_{22}+2F_{12}+$$

$$4F_{66})\int_0^a\int_0^b \frac{\partial^2 X_m}{\partial x^2}\frac{\partial^4 Y_n}{\partial y^4}X_mY_n\,dxdy+$$

$$J_{44}\int_0^a\int_0^b X_m\frac{\partial^4 Y_n}{\partial y^4}X_mY_n\,dxdy+J_{55}\int_0^a\int_0^b \frac{\partial^4 X_m}{\partial x^4}Y_nX_mY_n\,dxdy+$$

$$(J_{44}+J_{55})\int_0^a\int_0^b \frac{\partial^2 X_m}{\partial x^2}\frac{\partial^2 Y_n}{\partial y^2}{}_n\,X_mY_n\,dxdy\Big]$$